Development And Automation Of A SFG–FROG System With LabVIEW™

Institute for Experimental Physics

In cooperation with

MAX-PLANCK-GESELLSCHAFT
Fritz-Haber-Institut
Department of Physical Chemistry

October 2018

Master Thesis

written by

Frank Quadt

Reviewer: Prof. Dr. Martin Wolf, Fritz–Haber Institut Berlin
Prof. Dr. M. Giersig, Freie Universität Berlin
Dr. R. K. Campen, Fritz–Haber Institut Berlin

I will make you love physics
and your life will never be the same.

Prof. W. H. G. Lewin

Declaration

I, Frank Quadt, declare that this thesis titled, *Development And Automation Of A SFG–FROG System With LabVIEW^{TM}* and the work presented in it are my own. I confirm that:

- This work was done mainly while in candidature for a research degree at this University.
- If any part of this thesis has previously been submitted for a degree or any other qualification at this University or any other institution, this has been clearly stated.
- Where I have consulted the published work of others, this is always clearly attributed.
- Where I have quoted from the work of others, the source is always given. With the exception of those quotations, this thesis is entirely my own work.
- I have acknowledged all main sources of help.
- Where the thesis is based on work done by myself jointly with others, I have made clear exactly what was done by others and what I have contributed myself.

Signed:

Berlin, September 29, 2018

Contents

Summary

In this thesis a device was build up for determining the amplitude as well as the phase of an ultrashort infrared LASER pulse, a so–called SFG–FROG device. Here SFG stands for sum frequency generation and describes the creation of electromagnetic waves in the range of 690 nm and 740 nm with the help of the combination of a LASER pulse with 800 nm and an infrared LASER pulse between a wavelength range of 3000 nm and 12000 nm.
The detection of ultra short infrared pulses are challenging. This why there are practically quite no commercial detectors available. The used semi–conductor elements just covers a small wavelength range and are partially expensive. To create a low cost solution a nonlinear crystal was used to shift the "task" in the visible region. Available detectors are much more sensitive for visible light than for any other spectral regions due to their semi–conductor properties.
For the measurement a combination between a spectrometer and an autocorrelator was used. A so–called FROG system. FROG is an acronym and stands for "Frequency Resolved Optical Gating". A technique which was introduce by Prof. Rick Trebino first in 1991. This process uses a simple approach by scanning i. e. two different pulses over each other. At the same time the corresponding time shift between these pulses as well as the convolution of the electrical fields, the so–called FROG–trace, is measured spectroscopically.
For creation a SFG light signal, several boundary conditions have to be fulfill. On the one hand a nonlinear medium is needed which due to the nonlinear process is able to produce such a SFG light. In this thesis a silver–thiogallate crystal with the chemical equation of $AgGaS_2$ as well as a size of (5x0.5x5) mm was used. On the other hand this crystal has to fulfill a specific cutting angle, due to momentum– and energy conservation laws the so–called phase–matching angle. The silver–thiogallate crystal was choosen because of its transparency ability and broad wavelength region for infrared LASER pulses and as thin as possible to prevent disturbances of the infrared pulse.
The FROG–trace contains all information which are necessary to determine the amplitude and phase of both ultra short LASER pulses. With the help of a in LabVIEW™ implemented algorithm, the so–called "Principle General Component Projection–Algorithm", short PGCP, can this be done. Whereby here on the mathematical point of view the problem will be reduced to an eigenvalue problem whereas the algorithm is able to determine a bijective solution. In this thesis the PGCP–algorithm was implemented and analysed. With simulated data, partially disturbed gaussian pulses the reliability, the accuracy, the run–time duration as well as the run–time duration of the slowest element in the algortihm was investigated.

Zusammenfassung

In der hier vorliegenden Arbeit wurde ein Gerät zur Bestimmung der Amplitude als auch der korrespondierenden Phase von ultrakurzen Infrarotlaserpulsen aufgebaut, ein sogenanntes SFG–FROG Gerät. SFG steht hierbei für Summenfrequenzgeneration und beschreibt in der vorliegenden Arbeit die Herstellung einer elektromagnetischen Welle im Bereich von 631 nm bis 750 nm, welche aus der Kombination eines LASER Pulses der Wellenlänge 800 nm als auch dem eines Infrarotpulses im Bereich von 3000 nm bis 12000 nm. Um die Herstellung des SFG Lichtes zu gewährleisten, müssen mehrere Randbedingungen erfüllt werden. Man benötigt ein nichtlineares Medium, welches durch nichtlineare Prozesse in der Lage ist, ein solches SFG Licht zu produzieren. Dieses Medium ist in der vorliegenden Arbeit ein Silber–Thiogallat Kristall mit der chemischen Formel $AgGaS_2$ und einer Abmessung von (5x0.5x5) mm
Die Detektion von ultrakurzen Infrarotpulsen ist jedoch sehr herausfordernd Die benutzten Halbleiterelemente decken nur einen kleinen Wellenlängenbereich ab und sind sehr kostenintensiv. Um eine kostengünstige Lösung zu bekommen wurde ein nichtlinearer Kristall verwendet um, das zu detektierende Signal in den sichtbaren Spektralbereich zu verschieben. Die kommerziell verfügbaren Detektoren sind für sichtbare elektromagnetische Strahlung wesentlich sensitiver als für andere Spektralbereiche. Dies liegt nicht zuletzt an den Halbleitereigenschaften. Um die Amplitude als auch die korrespondierende Phase zu vermessen wurde eine Kombination zwischen Spektrometer und Autokorrelator verwendet. Ein sogenanntes FROG System. FROG ist ein Akronym aus den englischen Wörtern “Frequenzy Resolved Optical Gating”. Eine Technik, welche von Prof. Rick Trebino 1991 das erste Mal angewendet wurde. Diese Frequenz aufgelöste, optische Verschiebung nutzt ein einfaches Verfahren. Man nimmt z. B. zwei unterschiedliche Pulse und scanned den einen mit dem anderen ab. Dabei wird nicht nur die Verschiebung der LASER Pulse zueinander aufgezeichnet, sondern auch zeitgleich die durch die Überlappung der beiden elektrischen Felder resultierende, geformte Faltung, dem sogenannten FROG–trace, spektroskopisch aufgenommen. Der FROG–trace beinhaltet alle Informationen, welche man benötigt um die Amplitude als auch die Phase beider ultrakurzer LASER–Pulse zu bestimmen. Mit Hilfe eines in LabVIEW™ implementiertem Algorithmus, dem “Principal General Component Projection–Algorithm”, kurz PGCP, wird dies durchgeführt. Dabei wird auf mathematischer Ebene die zu Grunde liegende Aufgabenstellung auf ein Eigenwert–Problem zurückgeführt, wofür der eben erwähnte Algorithmus eine ein–eindeutige Lösung errechnet.
In der nachfolgenden Arbeit wurde der PGCP–Algorithmus implementiert und analysiert. Mit Hilfe von simulierten, teilweise gestörten, Gauß'schen Pulsen wurde die Verlässlichkeit, die Genauigkeit als auch die Geschwindigkeit, sowie das Geschwindigkeits limitierende Element im Algorithmus ermittelt.

Chapter 1

Motivation

Understanding nature is one of the key achievements, which physics is dealing with. Today, due to centuries of research and investigations we are capable to explain a huge amount of nature behaviour. We are going deeper and deeper into the smallest things ever observed such as in biology the process of photosynthesis or vision or how the protein–folding works as well as in chemistry we are able to see and investigate specific molecular vibrations, re–orientation and liquid–phase collisions.
Moreover, in physics specific lifetime of excited–states, photo–ionisation and electron–hole interactions are well understood. All of these mentioned processes can be observed with light. More specific with LASER pulses. Through the development of the LASER in the 1960s [16] the humanity is able to generate single pulses, which satisfies different properties, such as specific frequency and intensity.
Over the years these pulses became shorter and shorter. Today, even durations of a few femtoseconds are available. For understanding the above mentioned processes a good characterised LASER pulse is necessary. If it is known what is the input of the system and measure the outcome, one can conclude and determine what happens inside the system. Especially ultra broadband infrared pulses are of great interest. However, infrared pulses are distorted if they pass through a specific medium with a wavelength–dependent refractive index.
Furthermore, there are other challenges which have to be overcome. On the one hand it is the extrem short duration of the LASER pulse. In order to measure an event in time, one has to use a shorter one in order to freeze the action. However, using these pulses, called femtosecond LASER pulses, it is almost impossible for electrical systems to measure them.
On the other hand the intensity of these pulses is challenging. Especially, in this thesis the use of infrared pulses is a problem. Sensors which can detect such low intensities like those of the infrared LASER beams are very expensive. In this thesis an inexpensive and practical solution is developed to overcome these challenges.
This experimental setup is called Frequency–Resolved Optical Gating – short FROG – which will be introduced and explained.
In contrast to other applications the FROG–setup is easy to build. It has the possibility to measure every ultrashort LASER pulse. For that there are a lot of modifications available, such as a polarisation–gated FROG, a self–diffraction FROG, la GRENOUILLE[1] as well as a second–harmonic FROG, just to mention a few. Due to its easy setup and the ability to achieve high information of the corresponding pulses in combination with its strong 2D–phase–retrieval algorithm is the FROG setup one of the most efficient and cheapest experimental setups for LASER pulse characterisation.

[1] This is an acronym and stands for **G**rating **E**liminated **N**o–nonsense **O**bservation of **U**ltrafast **I**ncident **L**ASER **L**ight **E**–fields. Furthermore, it is the french word for frog.

Chapter 2

Theoretical Basics

2.1 And There Was Light: The LASER

The invention of the LASER in the middle of the 20 th century is one of the greatest in the history of science. What exactly is a LASER? What types are available? When should I use which LASER and how it is working in general? These questions and much more will be explained in the following chapter.

2.1.1 History And Definiton

Before we dive into the hugh field of LASER physics we should take a closer look to the development and meaning of a LASER. As you already may know the word LASER is actual an acronym and stands for **L**ight **A**mplification by **S**timulated **E**mission of **R**adiation. This acronym describes the creation process of such an intense light source. However, a much more detailed and correct definition is given below.

Definition 1 *A LASER is a device that makes use of processes that increase or amplify light signals after those signals have been generated by other means. These processes include the stimulated emission and the optical feedback. It produces a highly directional and high–intensity beam that most often has a very pure frequency or wavelenth.*[19]

2.1.2 Types of LASERs

In general, there are two different types available: a LASER which emit a continous wave (cw) and those which emit a pulsed LASER beam. Both can be separated into three subcategories: gas LASERs, dye LASERs and solid state LASERs.
Although the invention and development of the LASER is in its early state there are a huge amount of LASERs available. There are LASERs available for every spectral region known. There are ultraviolet–LASERs which can be used to investigate transistions between electron niveaus of molecules, infrared LASERs to i .e. investigate the rotational behaviour of molecules as well as LASERs in the visible range which can be used to investigate the absorption behaviour of molecules or solids available. Every type has its own individuel properties and usage for specific applications.
Gas LASERS are mostly operated with electrical gas discharges but also optical excited with CO_2–LASERs[1]. In comparison to that the dye LASERs and the solid state LASERs are optical pumped by using gas discharging lamps or other LASERs [7].
In Fig.2.1 an overview is presented which shows the different energy as well as wavelength regions of several LASER types. For a list of examples of LASERs with its emitted wavelength or wavelength region please take a look into Chapter 3 of [7].

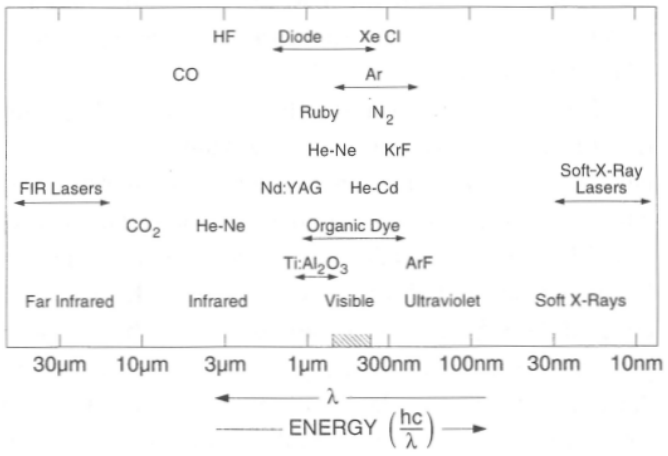

Figure 2.1
Picture with different kinds of LASERS and its range in the wavelength domain.[19]

[1] The CO_2–LASERs are the most used and most important LASERs used for industrical applications. It has a high power of quite up to 100 kW and an efficiency between 10 % and 20 % [7]

2.1.3 How a LASER is working

To understand how a LASER can produce or generate coherent electromagnetic radiation one can use two different approaches. On the one hand the semi–classical point of view and on the other the quantum mechanical one. For further investigations the semi–classical approach will be used in the next chapters.

Two–Level–Niveausystem

An atomic system consists of different quantized energy levels. A so–called two–level system will be used to explain the main concept of generating LASER radiation. For a better understanding we are simplify the atomic energy level structure by using just two different energy levels. The ground energy level which will be indicated by E_1 as well as an excited and therefore higher energy level indicated by E_2 will be used. One of the first steps is to assume that the whole system is in thermal equilibrium. For that one can further assume that the population of each energy level can be described by the Boltzmann distribution:

$$N_i = N_0 \cdot e^{-\frac{E_i}{k_B T}} \tag{2.1.1}$$

Moreover, for a complete understanding the so–called spectral energy densitiy $u(\nu, T)$ which is used to described the radiation field in dependence of the frequency as well as the temperature has to be mentioned here. However, due to the fact that we are assuming that the whole system is in thermal equilibrium the spectral energy density can be described by three theories in total. On the one hand the radiation law of Max Planck which is given by [5]:

$$u(\nu, T)\, d\nu = \frac{8\pi h\nu^3}{c^3} \cdot \left(e^{\frac{E}{k_B T}} - 1 \right)^{-1} d\nu \tag{2.1.2}$$

This equation is actual valid for black body radiation in thermal equilibrium whereas the size of the object has to be greater than the wavelength. For the limits of small frequencies the Rayleigh–Jeans–Law can be used [5]:

$$u(\nu, T)\, d\nu = \frac{8\pi\nu^2}{c^3} \cdot k_B \cdot T \cdot \, d\nu \tag{2.1.3}$$

Regretly, for high frequencies ν is diverging and results into the so–called ultra–violet catastrophe. The last equation of the mentioned three is an equation in limits of high frequencies, the displacement law of Wien [5]:

$$u(\nu, T)\, d\nu = \frac{8\pi h\nu^3}{c^3} \cdot e^{-\frac{E}{k_B T}} \cdot \, d\nu \tag{2.1.4}$$

Absorption Process

Like you may already know an atomic system can absorb a photon just with a specific quantified energy of $E = h \cdot \nu = \frac{hc}{\lambda}$ whereas ν is the corresponding frequency of the photon and h is Plancks contant.

Therefore, the corresponding incident photon has to be the exact energy which differs the energy levels E_1 and E_2 from each other. In other words: the energy difference between $\Delta E = E_2 - E_1$ (with $E_1 \leq E_2$) is necessary to put an electron from the ground state to the excited state indicated as "1" and "2" in Fig. 2.2 schematically respectivly. Here an incoming photon of a specific energy of $E = h\nu$ is absorbed and the electron uses this energy to go from the ground level to the excited state of this atomic system. Moreover, one can specify a probalitiy of absorbing such a photon in a time intervall dt. This was done by Albert Einstein first [20].

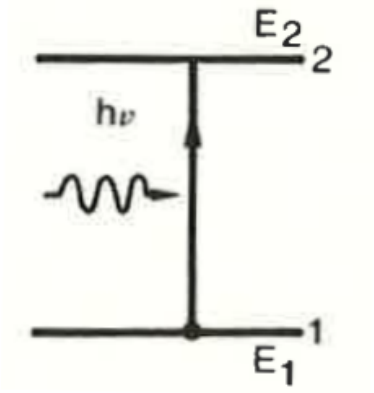

Figure 2.2
An energy level scheme of a two–level system which shows an absorption process [20].

In Equ. 2.1.5 the probability W_{12} for absorbing a photon and influence an electronto go from state 1 to state 2 is depending on the spectral energy density and the so–called Einstein–coefficient B_{12}.

$$dW_{12} = u(\nu) \cdot B_{12} \cdot \, dt \tag{2.1.5}$$

Further, in this time intervall dt a specific amount of atoms will do this state change. This change of the population density of the ground state can be expressed mathematically by:

$$\begin{aligned} dN_{12} &= N_1 \cdot \, dW_{12} && (2.1.6) \\ &= N_1 \cdot u(\nu) \cdot B_{12} \cdot \, dt && (2.1.7) \end{aligned}$$

Spontaneous Emission

With respect to the Boltzmann distribution some electrons are in the excited state E_2 if $T > 0$. These electrons can go down to the ground state again by emitting a photon with the energy $E_2 - E_1 = h\nu$. This process is spontaneous and independ from the external radiation field. However, one can specify an average life time τ_{sp} in the excited state. An important fact is that this spontaneous emission is arbitrary in the time intervall, the direction of the emittied radiation, a polarisation as well as the phase are also arbitrary. is shown schematically in Fig. 2.3.
Further, like for the absorption process, a probability can be given that an electron goes from the excited state to the ground state:

$$dW_{21}^{sp} = A_{21} \cdot \, dt \tag{2.1.8}$$

Here A_{21} is the Einstein coefficient for spontaneous emission. It is inverse proportional to the average life time: $A_{21} = \frac{1}{\tau_{21}}$.

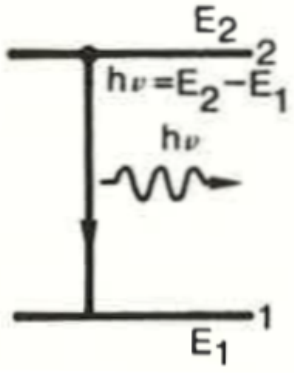

Figure 2.3
An energy level scheme of a two–level sytem which shwos a spontaneous emission process [20]

Stimulated Emission Or Induced Emmision

The stimulated emission is also called induced emission [5]. However, in contrast to the spontaneous emission the stimulated emission occurs just by the influence of an external radiation field like an electromagnetic wave which has an influence on the atomic system.
This process describes an electron which is already in the excited state E_2 but is influenced by an external electromagnetic field to go down to the ground state E_1 by emitting a photon with an energy of $E_2 - E_1 = h\nu$ [5, 20]. The important fact is that the induced emitted photon has a definite phase relation to that of the incident one. That means in the case of the stimulated emission, due to the fact that this process is forced by an incident photon, the emission of such a photon occurs in the same direction. In contrast to that of the spontaneous emission which can be emitted in any direction [20]. This is the key aspect to produce a LASER system.

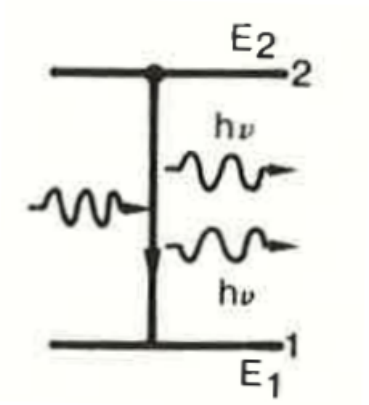

Figure 2.4
An energy level scheme of a two–level system which shows a stimulated emission [20].

However, as a last note I have to mention that the just described processes are one of to possible ways for the atom or the molecule to decay. There is an other possibility for a so–called nonradiative decay. In this case the energy difference $\Delta E = E_2 - E_1$ can be delivered in some form of energy other than the above mentioned electromagnetic radiation. These energy may go into the inernal energy of the surrounding atoms or molecules or into the kinetc [20].

2.2 Ultrashort LASER Pulses

2.2.1 Pure Or Idealized LASER Pulses

Since the invention of the LASER in the mid 1960s by Franken [16] a hugh amount of applications and devices were developed. LASER is an acronym for Light Amplification by Stimulated Emission of Radiation, which describes the concept of generating LASER light. At the moment, two different types of LASERs can be distinguished.
On the one hand are the pulsed LASERs and on the other hand are the continuous wave[2] LASER. The main difference between these two types is the kind of propagation of the generated light. While the continous wave LASER generates an electromagnetic wave with constant frequency and amplitude, which can be mathematical described by a cosine–shaped function, the pulsed LASER emits a short electrical burst or flash of light which contains a specific frequency range enveloped by a corresponding mathematical function. Therefore, one possible definition is:

Definition 2 *An ultrashort LASER pulse is a very short burst of electro–magnetic energy which can be described by its electric field as a function of space and time,* $\vec{E}(\vec{r}, t)$ *[22].*

For describing the corresponding shape of the ultrashort LASER pulse two different possibilities are available. These are the time–domain as well as the frequency–domain.
In Fig. 2.5 a typical pulse in the time–domain is shown. Noticeable are the specific values within this curve. At all other times the values are close to zero. The corresponding pulse width is often defined as the full width at half maximum (FHWM) as it is shown in Fig. 2.5. Such a pulse can be obtained by multiplying a specific function with an envelope. This infrared pulse can be mathematical described by the following equation:

$$E(t) = \cos[\omega t] \cdot e^{-\frac{\omega_0^2}{2\Delta^2}} \tag{2.2.1}$$

With t the time and Δ the standard deviation as well as ω_0 is the corresponding central angular frequency.

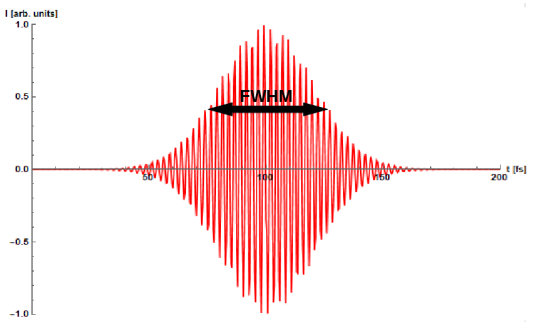

Figure 2.5
An idealized ultrashort pulse with a FWHM width of approx. 100 *fs*

[2] In the following a closer look to the pulses instead of the continous waves will be taken due to the importance referring this thesis.

Here the corresponding envelope is a gaussian function. Furthermore, one can recognize the phase dependency. Another important fact is that the angular frequency has a time–dependence which depends also on the phase ϕ and is important to understand chirped pulses, of the form:

$$\omega(t) = \omega_0 + \frac{d\phi}{dt} \tag{2.2.2}$$

After mention how a LASER pulse looks like in the frequency domain the question arises how such a pulse looks like in the time domain.

As an interesting fact the time domain can be determined by using the frequency domain values and using the fast Fourier transformation.

$$E(t) = \int_{\infty}^{-\infty} E(w)e^{i\omega t}\, dt \tag{2.2.3}$$

This is also possible by using the other direction as well by using the following equation:

$$E(w) = \int_{-\infty}^{\infty} dt E(t) \cdot e^{-i\omega t} \tag{2.2.4}$$

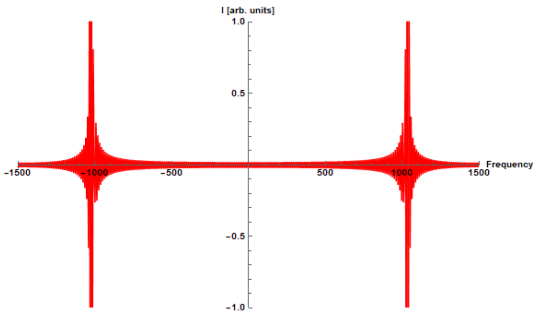

Figure 2.6
Scheme of an ultrashort LASER pulse in the frequency–domain. Notice the two sharp peaks in total which occurs due to the negative values of the integral of the Fourier transformation.

In Fig. 2.6 is shown the fast Fourier transformation of the same pulse which is displayed in Fig. 2.5. Note the sharp peaks in the time–domain but in the frequency–domain the pulse is broad. This can be explained by the energy–time uncertainty:

$$\Delta E \Delta t \geq \frac{\hbar}{2} \quad \text{with} \quad \Delta E = \hbar \Delta\omega \tag{2.2.5}$$

$$\Rightarrow \Delta\omega \Delta t \geq \frac{1}{2} \tag{2.2.6}$$

That means, the sharper the pulse is in time the broader is the pulse in the frequency–domain and contains more specific frequencies.
However, the last two examples of an ultrashort pulse in the time– as well as frequency–domain are idealised. Regretly, no ultra short LASER pulse has such a shape in the real world as all are influenced by their environment. Especially, the infrared pulse can be influenced by the surrounded air by absorption.

Further, one of the main issues, is that a pulse is a package of several different frequencies. By passing through a medium the group velocity of this pulse is changing. Some frequencies will be slowed down other will speed up depending on the mentioned wavelength–depended refractive index of the medium. Therefore the corresponding pulse change its shape and will be called chirped. This is due to the previous mentioned time–dependence of the angluar frequency $\omega(t)$ (see Equ. 2.2.2).

2.2.2 Chirped Pulses

In the previous sections an idealized, gaussian shaped and ultrashort LASER pulses was described in general. However, this model cannot describe the influenced referring the different fequencies which a LASER pulse is consisting of.

These influences with respect to time are called chirp. Therefore, a chirped pulse is a LASER pulse which changes the individual propagation velocities of the containing frequencies. Ergo: The beginning frequency of a LASER pulse differs from one than at the end of the pulse. In the laboratory these disturbance results in the absorption process in fluids or not proper transmission through the electronical devices.
Furthermore, there are several types of chirped pulses like linear positive or linear negative ones.
As an example, in the mathematical point of view, a linear chirp can be expressed by introducing a time dependence to the angular circular frequency.

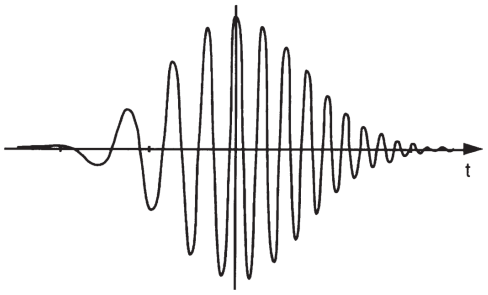

Figure 2.7
An idealized gaussian chirped pulse [17]. Notice the slower frequencies at the beginning and the fasten frequencies at the end of the pulse.

Therefore the now time dependent angular frequency velocity changes to:

$$\omega(t) = \omega_0 + \text{linear disturbance} \tag{2.2.7}$$

in such a way that the idealized gaussian shaped undisturbed electrical field equation (refer to Equ. 2.2.1) is changed to:

$$E(t) = \cos\left[\omega(t) \cdot t\right] \cdot e^{-\frac{\omega_0^2}{2\Delta^2}} \quad \text{with} \quad \omega(t) = \omega_0 + k \cdot \pi \cdot t \quad \text{and} \quad k = \frac{f_{end} - f_{start}}{T} \tag{2.2.8}$$

Take attention to the frequency values f_{start} as well as f_{end}. These values describing the start frequency and the end frequency of the given pulse and T describes the time intervall in which the start frequency is changing to the end freqeuency. In other words, it describes how fast the frequency is changing from one to the other value.

2.3 Frequency Resolved Optical Gating (FROG)

2.3.1 The Story Of FROG

Ultra short pulses as well as their small time scale are very important in many areas of the scientific world. Such pulses are necessary to investigate important processes, like protein folding, re–building of the retinal protein which is necessary for our vision or chemical reactions in general. Just these electrical bursts of energy are capable to achieve the necessary time resolution to investigate these processes.
As mentioned in the motivation part it is necessary to get the full information of the pulse by characterizing it. However, how can we measure the shortest event ever created?
The answer is easy: The shortest event available for measuring the pulse is the pulse itself [22]. For that a class of techniques was introduced by Daniel J. Kane and Rick Trebino in 1992. These special technique is the **F**requency–**R**esolved **O**ptical **G**ating, in short: **FROG**.
Before the invention of the FROG techniques it was not possible to measure the intensity of a pulse vs. time as well as phase of the pulse vs. time without achieving blurry pictures [22]. However, Prof. Trebino and Daniel Kane solved these problems with its special technique. It can measure the full time–dependent intensity and phase of ultrashort LASER pulses in a wide variety of circumstances [22]. This device can be seen as a combination of an autocorrelator and a spectrometer which results into such powerful properties.

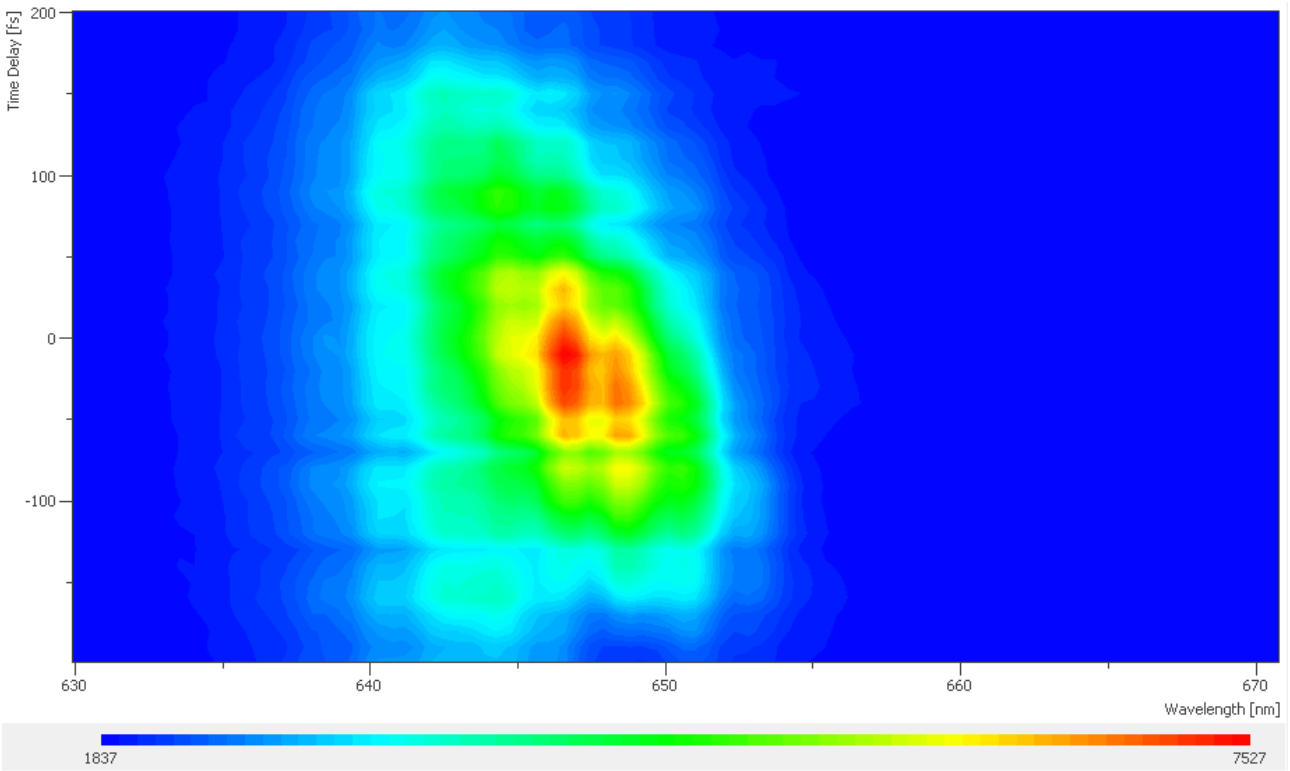

Figure 2.8
A typical FROG–trace which was obtained by overlapping two different pulses of wavelengths of 800 *nm and* 4000 *nm in a nonlinear crystal. Through nonlinear processes a sum frequency LASER beam was generated.*

2.3.2 FROG At Work

The FROG technique is using a combination of the time– as well as the frequency–domain, the so–called time–frequency–domain. However, this intermediate or mix domain is not new. It is widley used in subjects like acoustics and applied mathematics. The obtained spectrum can be written in its mathematical form as [22]:

$$\Sigma_g^E(\omega,\tau) = |\int_\infty^\infty dtE(t)g(t-\tau)e^{-i\omega t}|^2 \tag{2.3.1}$$

Whereas $g(t-\tau)$ is a variable gate function and $E(t)e^{-i\omega t}$ is the electric field of a specific pulse. Therefor the frequency–resolved optical gating method measures a spectrogram of the pulse. However, it cannot use available spectrogram inversion algorithm [22] due to the fact that both the pulse as well as the replica which is just a copy of the previously mentioned pulse is also not known.
FROG is in its simplest form any autocorrelation–type measurement in which the autocorrelator signal beam is spectrally resolved [22].
But instead of measuring energy vs . time which occurs by an autocorrelator one measures the spectrum dependent of the delay time of the gate pulse, the so–called FROG–trace[3].
From this trace one can calculate the shape of the pulses which were used. This is possible due to a 2D–phase–retrieval algorithm. Such an algorithm is the principal component generaliyed projection which will be explained in detail in chapter 2.4.

[3] This kind of spectrum is also known as Wigner–diagram

2.3.3 Sum Frequency Generation

In the last chapter a closer look to the mathematical description of an idealised ultrashort pulse and how as well as why it is influenced by media was taken.
To summarize there are two main facts which prevents to determine ultrashort infrared pulses. First, the sensitivity of these pulses. As you may already know infrared pulses are strongly influence by different media and will be, freqency depended, absorbed by air. Furthermore, it will be overlapped with another pulse of 800 nm wavelength. Therefor the corresponding intensity is extremly weak. Moreover, devices which can detect infrared pulses are extremly expensive.
A more simpler way to combine both the economic and the intensity challenge is to use a sum frequency generation beam. This beam is a second order nonlinear process with specific properties. On the one hand a sum frequency generation beam (SFG) has a wavelength range[4] from $0.63\mu m$ up to $0.75\mu m$. The wavelengths are quite easier to detect than the IR beam range of $3\mu m$ up to $12\mu m$ due to the fact that the commercially available detectors are much more sensitive for the visible region.
On the other hand the SFG is much easier to achieve than other nonlinear processes and the intensity is due to the second order susceptibility in the order of 10^{-12}. A third order susceptibility is of the order of 10^{-24} [2]. A huge difference!
However, before starting to deal with a SFG beam in this chapter the basics of the nonlinear optics as well as especially the sum frequency generation will be described. One of the first questions we have to be consider is what exactly is nonlinear optics about and how it differs from the linear optics?
The development of the nonlinear optics field started with the discovery of the so–called second–harmonic generation by Franken et al. in 1961 [16]. This was only possible because the LASER was invented by Maiman in 1960 [11].
There are a lot of definitions what nonlinear optics is. Here is one of the best:

Definition 3 *Nonlinear optics is the study of phenomena that occur as a consequence of the modification of the optical properties of a material sytem by the presence of light [2].*

At first, there is to consider the question: what is the difference between linear and nonlinear optics?
In linear optics light induces in matter a polarisation $\vec{P}$, which is dependent on the electric field $\vec{E}$ in a linear way:

$$\vec{P} = \epsilon_0 \cdot \chi \cdot \vec{E} \tag{2.3.2}$$

Here χ is the electric susceptibility of the influenced medium and ϵ_0 the permittivity of the free space. However, if the electric field of the incident beam becomes strong this linear approximation is not valid anymore and higher terms have to be considered as indicated by the numbers in brackets in Equ. 2.3.4.

[4] Here I assume a combination of a $0.8\mu m$ and an infrared beam in the range from $3\mu m$ up to $12\mu m$

For that, the polarisation $\vec{P}$ can be used with the Taylor series of the form [10, 18]:

$$\vec{P} = \vec{P}^{(1)} + \vec{P}^{(2)} + \vec{P}^{(3)} + \dots \tag{2.3.3}$$

$$= \epsilon_0 \cdot \chi^{(1)} \cdot \vec{E} + \epsilon_0 \cdot \chi^{(2)} \cdot \vec{E}^2 + \epsilon_0 \cdot \chi^{(3)} \cdot \vec{E}^3 + \dots \tag{2.3.4}$$

Whereas $\chi^{(1)}$ is the scalar, linear susceptibility. Every other higher terms of $\chi^{(i)}$ are the i–order susceptibility of tensor form. In this thesis a nonlinear optical process of second order will be used – the sum frequency generation (SFG). Like all $\chi^{(2)}$–processes it is forbidden in media with inversion symmetry [10, 18].
For that consider two incident LASER beams of the form $E_1(t) = E_1 \cos[\omega_1 t]$ as well as $E_2(t) = E_2 \cos[\omega_2 t]$. If these beams overlap in space and time in or on a medium with broken inversion symmetrie they induce a second order polarisation $\vec{P}^{(2)}$ of the form:

$$\vec{P}^{(2)} = \epsilon_0 \chi^{(2)} \cdot \left(E_1 \cos[\omega_1 t]\, \hat{e_1} + E_2 \cos[\omega_2 t]\, \hat{e_2}\right)^2 \tag{2.3.5}$$

After applying the binomial formular and with

$$\cos[x] \cdot \cos[y] = \frac{1}{2}(\cos[x+y] + \cos[x-y]) \quad \text{as well as} \tag{2.3.6}$$

$$\cos[x] = \frac{1}{2}(1 + \cos[2x]) \tag{2.3.7}$$

one can rewrite equation 2.3.5 in the following form:

$$\vec{P}^{(2)} = \frac{1}{2}\epsilon_0 \chi^{(2)} \left[E_1^2(1 + \cos[2\omega_1 t]) + E_2^2(1 + \cos[2\omega_2 t])\right] + \epsilon_0 \chi^{(2)} \left\{ E_1 E_2 \cdot \hat{e}_1 \hat{e}_2 \cdot \left(\cos\left[\underbrace{(\omega_1 + \omega_2)}_{\text{SFG}}\, t\right] + \cos\left[\underbrace{(\omega_1 - \omega_2)}_{\text{DFG}}\, t\right] \right) \right\} \tag{2.3.8}$$

After these calculation equation 2.3.8 shows that the polarised media itself can act as a light source due to its nonlinear process [10]. According to this equation the medium can emit light at frequencies of $2\omega_1$, $2\omega_2$, $\omega_1 + \omega_2$ as well as $\omega_1 - \omega_2$. These emitted light frequencies correspond to multiple nonlinear processes namely: seconde harmonic generation (SHG, 2ω), difference frequency generation (DFG,$\omega_1 - \omega 2$) and sum frequency generation (SFG,$\omega_1 + \omega_2$). In the following the focus will be on the SFG process only.

The sum frequency generation is one nonlinear processes which can be observed only by using a high intensity light beam. To achieve this a LASER beam is necessary as this beam is the only one which has the corresponding intensity to achieve a non–neglecting second order process. Furthermore, the corresponding medium has to have a non–inversion symmetry which is achieved by its crystal structure or due to a symmetry broking surface. However, a nonlinear second order process cannot happen if the medium has inversion symmetry. This will be clear if one assume a crystal with inversion symmetry. In case of such a crystal the medium has to be symmetric by $x \to -x$. By taking a closer look to the induced polarisation – but just the second order one – one yields:

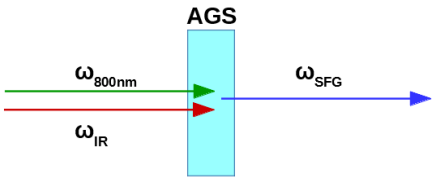

Figure 2.9
Schematically process for obtaining SFG by overlapping a 800 *nm and an IR LASER beam in space and time in a silver thiogallate crystal (AGS)*

$$\vec{P}^{(2)} = \epsilon_0 \chi^{(2)} \vec{E}^2(t) \tag{2.3.9}$$

If we change the sign of the incoming electromagnetic field the polarisation has to change its sign, too [10]. So we get:

$$-\vec{P}^{(2)} = \epsilon_0 \chi^{(2)} \cdot \left(-\vec{E}^2(t)\right) \tag{2.3.10}$$

The only way equation 2.3.9 and equation 2.3.10 can be fulfilled is, if $\chi^{(2)} = 0$. Therefore the used silver thiogallate crystal has necessarly a non–inversion symmetry.
Moreover, how can we determine the exact wavelength of the produced SFG LASER beams? For that we will use the energy conservation law of the form:

$$E_{800nm} + E_{IR} = E_{SFG} \quad \text{with} \quad E = \hbar\omega \tag{2.3.11}$$

$$\Rightarrow \omega_{800nm} + \omega_{IR} = \omega_{SFG} \quad \text{with} \quad \omega = 2\pi f \quad \wedge \quad c = \lambda f \tag{2.3.12}$$

$$\Rightarrow \frac{1}{\lambda_{800nm}} + \frac{1}{\lambda_{IR}} = \frac{1}{\lambda_{SFG}} \tag{2.3.13}$$

$$\Rightarrow \lambda_{SFG} = \frac{\lambda_{800nm} + \lambda_{IR}}{\lambda_{800nm} \cdot \lambda_{IR}} \tag{2.3.14}$$

Also the moment has to be considered. For that the following equation has to be fulfilled:

$$\vec{k}_{800} + \vec{k}_{IR} = \vec{k}_{SFG} \tag{2.3.15}$$

Both the energy conservation law as well as the moment conservation law has to be fulfilled to obtain SFG. This is also called the phase matching condition. This calculation results to a specific angle value in which the crystal has to be oriented to achieve a SFG production.
A detail calculation of this phase matching angle is shown in appendix B.

2.4 The Principal Component Generalized Projection

The principal component generalized projection (PCGP) was first developed as well as published by Daniel J. Kane in 1998 [8]. While the FROG setup is simple the necessary determination of the intensity and phase of the measured pulse can be slow. The PCGP algorithm is using a mathematical process, the so–called single value decomposition, which change the problem to an eigenvalue determination. However, this decreases the time for calculation enormously.
In the following the PCGP algorithm will be explained in a more detailed way.
First of all, it needs some assumption of how both pulses would look like. For that there is only two restrictions: both have to be a non–zero vector with the same dimension N. This is just to give the algorithm some starting point. The real pulse shape will be determined by the PCGP algorithm.
As one of the first steps the outer product M_{outer} from both pulses will be build. The outer product gives us a matrix M^{outer}_{assume} which represents the convolution of the electric field $\vec{E}(t,\tau)$ of both pulses. However, to achieve an equivalent matrix[5] one can rotate the rows. This is necessary to retain the rank of the matrix but by rotating the rows one obtain the right time–domain.
The first row will not be touched. But the next one will be shifted to the left about one value, the second about two values and so on. So that every row is shifted by $n-1$ whereas n is the row number. So the matrix M^{outer}_{assume} change its shape as:

$$M^{outer}_{assume} = \begin{pmatrix} m_{11} & m_{12} & \dots & m_{1n} \\ m_{21} & m_{22} & \dots & m_{2n} \\ \vdots & \vdots & \vdots & \vdots \\ m_{m1} & \dots & \dots & m_{mn} \end{pmatrix} \tag{2.4.1}$$

$$\rightarrow M^{outer}_{rotate} = \begin{pmatrix} m_{11} & m_{12} & \dots & \dots & m_{1n} \\ m_{22} & m_{23} & \dots & m_{2(n-1)} & m_{21} \\ \vdots & \vdots & \vdots & \vdots & \vdots \\ m_{mm} & \dots & \dots & m_{m(m-n-1)} & m_{m(m-n)} \end{pmatrix} \tag{2.4.2}$$

[5] From the mathematical point of view an equivalent matrix is a matrix with the same rank: $rg(\mathbf{A}) = rg(\mathbf{B})$ [13]

By taking a closer look to the colums one recognizes that every column represents the overlapping electrical field of the 800 nm pulse as well as the time delayed gate–pulse.
So the first column represents the probe pulse multiplied by the gate pulse without a time shift whereas the second column displays the convolution with a time delayed gate–pulse [22].
After that the fast Fourier transformation will be used to obtain the complex form of the rotated matrix in the frequency domnain. Then the algorithm splits the individual values into its real and imaginary part to remove and replace the just calculated amplitude with the measured one which one had obtained from the experiment. Now the algorithm goes backwards and is doing an inverse fast Fourier transformation, re–rotate the matrix and then it is doing the single value decomposition. The single value decomposition decomposes a matrix into a superposition of outer product of vectors of the form [4]:

$$\mathbf{A} = \underbrace{\mathbf{U}}_{\text{probe}} \times \underbrace{\mathbf{W}}_{\text{weights}} \times \underbrace{\mathbf{V}^T}_{\text{gate}} \tag{2.4.3}$$

Whereby $\mathbf{U}$ and $\mathbf{V}$ are orthogonal and the columns are orthonormal to each other and $\mathbf{W}$ is a diagonal matrix.
Such a decomposition can always be done and the solution is almost unique [4]. The result of the SVD is – in our case – the possible pulse matrix $\mathbf{U}$ and gate matrix $\mathbf{V}$ weighted by $\mathbf{W}$. For physical sensful reasons we are interessted in the first position of $\mathbf{W}$ which is the highest value. All other possibilities and weights will be neglected and just the first column of $\mathbf{U}$ and the first row of $\mathbf{V}$ will be used for further calculation to obtain an even better result (if there is one).

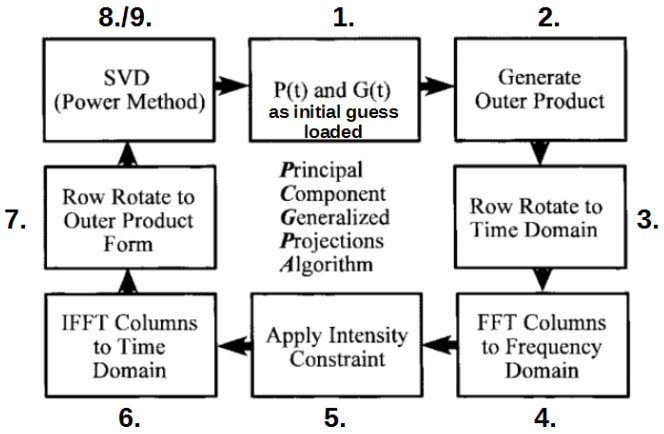

Figure 2.10
Scheme of the working process of the PCGP–algorithm. After the initial guess was used to generate the outer product a FFT was done. By replacing the magnitude of the calculation by the measured FROG trace magnitude and do an inverse FFT a single value decomposition determine the next guess for the measured ultrashort pulses.
The different steps are indicated by the numbers and will be explaint in detail in Sec. 3.2 [22]

Chapter 3

The PCGP–Implementation In LabVIEW^{TM}

3.1 The Programming Language LabVIEW^{TM}

LabVIEW^{TM} is an acronym and stands for **Lab**oratory **V**irtual **I**nstrument **E**ngenieering **W**orkbench. It was introduced by National Instruments in 1986 and is one of the most used programm languages in industry and science in today. Main reason for that is that it provides widley possibilities to acquire data, control devices and evaluate the data itself too.

Figure 3.1
One of the Logos of the programming language LabVIEW^{TM} [1]

This programming language differs from the usually used programming languages like C++, Haskell, Java or even ProLog. Instead to be an imperativ, functional or a logical programming language LabVIEW^{TM} is a pure graphical programming language. It is also using the so called data flow principle where the data flow controls the chronology of data processing. For that the different data typs like boolean, integer, strings or arrays are represented as wires which are connected to different icons. These icons are either specific functions, e.g. mathematical functions, or subprograms. These made the programming tasks much more easier and reduce the time of development due to its possibility to modularity and reusability.

Furthermore, the LabVIEW^{TM} develope environment has a clear structure. It is separated into two different windows, the front panel as well as the block diagram respectivley. The front panel is used to design the user interface of the application. This can be made via drag and drop of the different controls, indicators and other necessary graphical elements or containers. In contrast to that the block diagram shows the source code of the application. In this panel the different controls, indicators as well as the different algorithms will be implemented. A typical source code and front panel with its documentation of LabVIEW^{TM} are shown in Fig.3.3 and Fig. 3.2 respectivley. The reader can convince himself/herself, that this kind of a source code is much more intuitiv then a normal source code written in any imperativ, functional or logical programming language.

The front panel window (Fig. 3.2) shows an example for determine the power of a matrix specified by the user. Remarkable is the easy and clear pattern of the user interface which was build with drag and drop. Something which is not easy achievable by using other programming languages like the above mentioned ones.

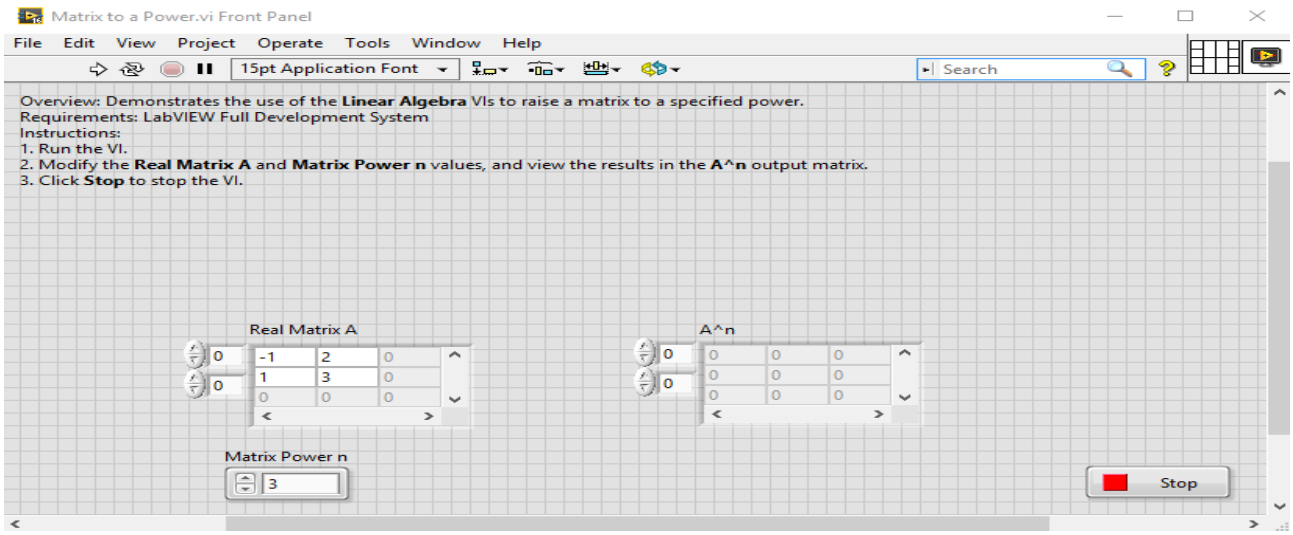

Figure 3.2
Typical front panel window of LabVIEW™ (obtained from an example bundle of LabVIEW™). Take attention to the clear user interface which was created by using drag and drop. This is not easy achievable using other programming languages.

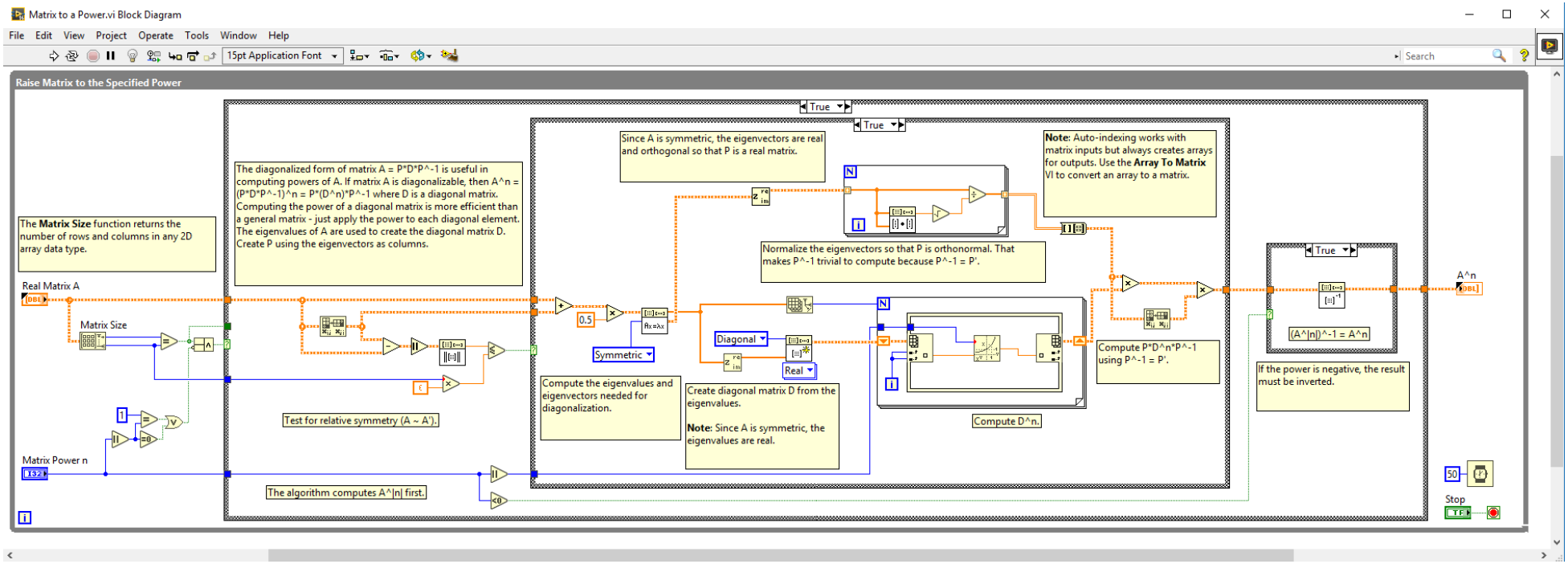

Figure 3.3

Typical source code written in LabVIEW™ which can be reviewed in the so–called block diagram window (obtained from an example bundle of LabVIEW™). Note the clear structure as well as the chronology which is influenced by the difference coloured wires. Further, a clear documentation or short comments can be given by using the yellow boxes.

3.2 The PCGP–Algorithm Implementation

Like mentioned in the previous sections LabVIEW™ was choosen due to its simplicity and modularity for implementing the corresponding principal component generalized projection algorithm which was described in detail in section 2.4.
For the ease of understanding the PCGP–algorithm implementation will be explaint step by step That means a closer look to the seven different moduls and/or functions will be done. In the folllowing all of the used functions of the PCPG–algorithm will be described shortly. Moreover, in Fig. 3.4 the source code of the algorithm is shown with its corresponding functions, indicated by their number.

1) **Load Data** Necessary to obtain the first guess as a starting point. Further, the measured FROG trace will be loaded. Notice that all of the loaded data has to be in a TDMS[1] file format otherwise an error will be given.

2) **Outer Product** The outer product function calculates the convolution of the electrical field of the given pulses.

3) **Row Shifting** For achieving the right time relation a shifting of the rows by using a specific pattern is necessary. This pattern was already described in section 2.4

4) **Calculation of FFT** This function determines the fast Fourier transformation and generates with the row shifting function a FROG trace from the given pulses. After that a complex matrix have to be handled by replacing the magnitude by the measured FROG trace one.

5) **Amplitude Constraint** Here the magnitude of the calculated FROG trace from the initial guess will be replaced by the measured one. The phase will be untouched.

6) **Calculation of IFFT** After the magnitude was replaced the algorithm goes backwards by using the inverse fast Fourier transformation as well as a reshift of the rows to achieve an outer product again.

7) **Re–Shifting Rows** Here the corresponding rows will be re–shifited to achieve the same structure as before.

8) **SVD or Power Method** The just calculated outer product which contains the phase of the determined FROG trace as well as magnitude is now put into the single value decomposition. Here this matrix will be handled like an eigenvalue problem and these pulses will be calculated which had produces the measured FROG trace. Moreover, due to improvement of the determination process of these pulses a much faster process, the so–called power method, can be used. This function reduces the eigenvalue problem to a normal matrix determination.

9) **Save Data with Time** Here the results of the calculated p– as well as g–pulse will be saved with respect of the current date and time.

.

[1] The **T**echnical **D**ata **M**anagement **S**treaming file format was introduce by National Instruments to achieve a fast data storing including meta data. Most other file formats like binary or ASCII ones are struggling with lost of meta data which can create unmeaningful data

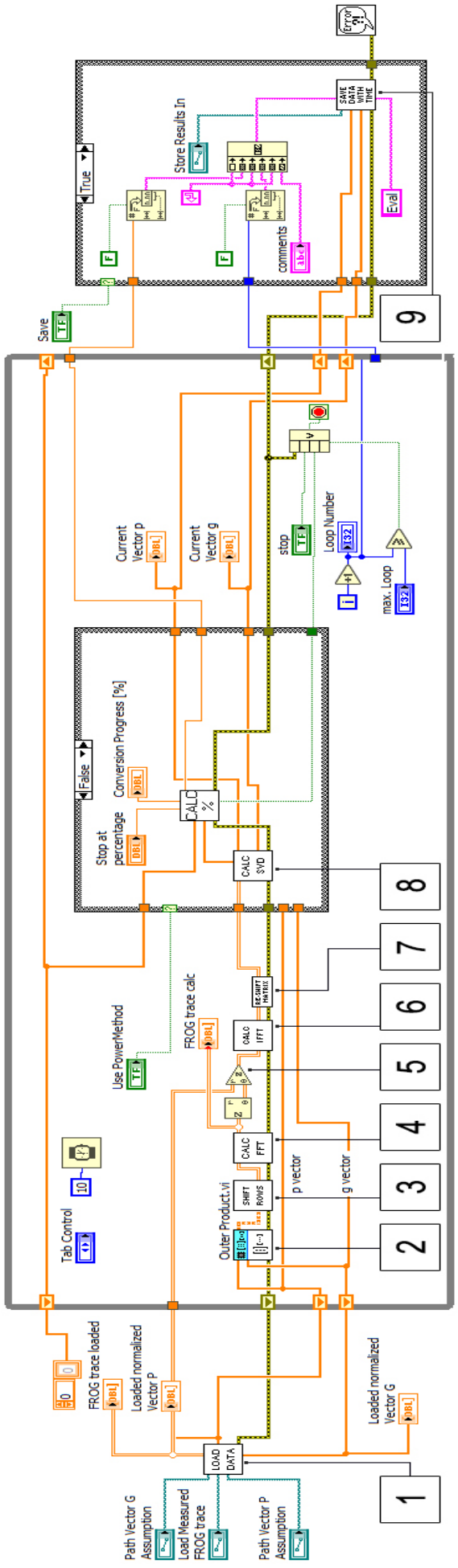

Figure 3.4

Source code of the PCGP–algorithm. Notice the numbers which indicates the previous mentioned used functions and its purpose.

Chapter 4

Analysing The Sensitivity Of The PCGP–Algorithm

In the following the PCGP–algorithm will be analysed referring its sensitivity and reliability. For that different gaussian shaped pulses were simulated. Pulses with and without gaussian white noise. Moreover, also complete FROG–traces were simulated with and without gaussian white noise.
After generating the corresponding pulses and FROG–traces the corresponding data were put into the PCGP–algorithm to obtain the phase as well as intensity relation of the pulses.
Further, a run duration analysis was done with respect to the accuracy of the corresponding algorithm. For that, a special test algorithm was invented to investigate the calculation speed in dependence of growing matrix size. Moreover, the limiting elements of the PCGP–algorithm were isolated. These bottle necks slowing down the whole application.

4.1 Simulation Of Different Pulses

4.1.1 Pure Gaussian Pulses

For analysing the corresponding algorithm different pulses which differs in length were simulated. Further, these pulses were put into the FROG algorithm.
Furthermore, I have to mention that I did three different calculation approaches in total. At first I simulated a FROG–trace with $\vec{p}(t)$ and $\vec{g}(t)$. After that I tried the FROG algorithm by putting $p(t)$ and $g(t)$ as a first assumption which results in the most fastes method. However, I also tried to just put $p(t)$ twice into the algorithm and after that I put $g(t)$ twice as the first assumption. All three process have an impact on the time for achieving the right result. The results are shown in Tab. 4.1.

Table 4.1
Time behaviour of the PCGP–algorithm in dependence of different lengths. Further, the corresponding right result which is determined by the algorithm against the time is dependend on the correct order of the initial guess.

	$\vec{p}(t)$ and $\vec{g}(t)$	$\vec{p}(t)$ and $\vec{p}(t)$	$\vec{g}(t)$ and $\vec{g}(t)$
Data Points	time [ms]	time [ms]	time [ms]
200	18	3030	3046
500	71	11679	11782
1000	505	68981	63852
1500	2126	243717	242739
2000	5559	480660	394484
3000	19990	3112170	2868335

In Tab. 4.1 are different pulse length listed. Each row of the table representing one run of the PCGP–algorithm. Every column represents the constellation of the given input as the first assumption of the PCGP–algorithm. Notice that the determination time of the corresponding constellations differs enormously depending on the given input. The given FROG–trace was the combination of the $p(t)$ and $g(t)$ pulse which are shown in Fig.4.1. These pulses were undisturbed, gaussian shaped pulses. The determination time increases rapidly if the used pulses were longer and do not fit to the right order as well as differs in phase and intensity. All of these properties have an influence of the run–time duration and of the success of the PCGP–algorithm.

A good assumption is necessary to obtain a result in general on a fast level. If the first assumption is to far away from the real going to determined pulses the PCGP–algorithm takes a long time to calculate the right result. Therefor it is also possible that the algorithm cannot find any result. If this happens a change in the order of the pulses or choosing another shape and intensity of the first assumption can be a part of the solution.

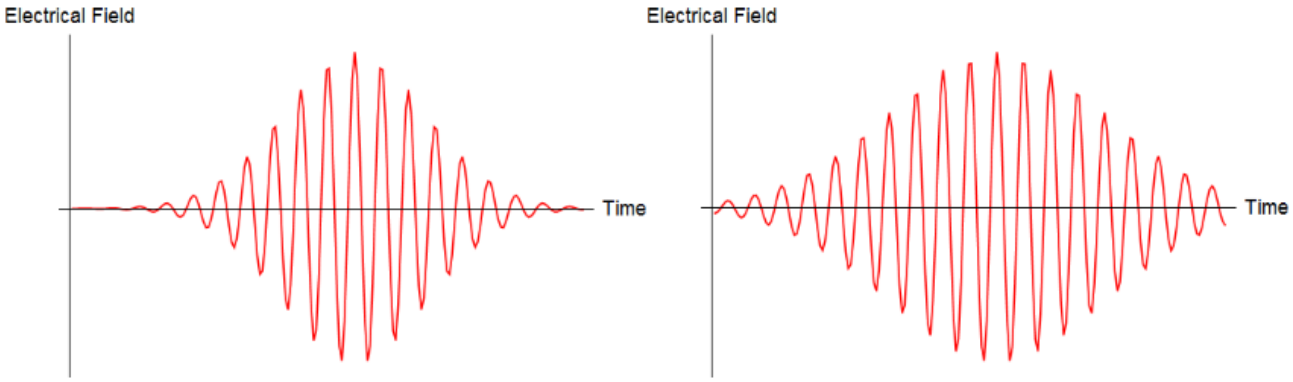

Figure 4.1
Two idealized, non–pertubated, gaussian pulses. On the left side the $p(t)$–pulse and on the right side the $g(t)$–pulse is shown.

4.1.2 Disturbed Gaussian Pulses

After we took a detailed look to the behaviour of the implemented FROG algorithm with pure gaussian pulses I want now take a closer look to the results given by using disturbed pulses. However, before we dive into this topic I should mention some words about disturbances in general. This is done in the following paragraph.

Kinds Of Noise

In the real world outside of the pure laboratory environment the measured pulses and or FROG traces can be disturbed.
These disturbances come from electronical interferences, scattered light which falls onto the CCD–chip or they occur due to the nonlinear effects which happens in the nonlinear crystal to create such short pulses. These disturbances result in noise which appears in the measured signal. Today plenty of noises are known, such as uniform gaussian noise, periodic random noise, inverse frequency noise or flicker noise, gamma noise, poison noise as well as binomial noise. Some are very known other needs additional research. TJhe most important sources of disturbances compared to the other ones is the white gaussian noise, Therefor in this thesis the main focus is the gaussian white noise. Other kinds of noises have not been considered.

White Gaussian Noise

Before we start to investigate the different ultrashort LASER pulses it is necessary to understand what is white gaussian noise.
The white gaussian noise is also called additve white gaussian noise. This term is widley used in information theory. There the white gaussian noise is used to mimic random effects which can occur during measuring data and transfering them.
Further, it is called white due to the fact it has an uniform power across the corresponding use frequency range. Moreover, it is gaussian distributed over the whole picture. These values can be added to a simulated signal to mmimic disturbances which occur in nature. White gaussian noise occur naturally and is generated or produced by e.g. thermal vibrations of atoms in conductors and black body radiation from earth.

Gaussian Pulses With Disturbed Cosine

In the following the idealized, gaussian shaped ultrashort LASER pulse was influenced by adding different varying gaussian white noise. However, not the whole pulse was influenced. Just the cosine term in the equation was changed in such a way that the oscillations were influenced. Therefore, the equation which describes the electrical field of such an ultra short pulse

$$E(t) = \cos\left[\omega t\right] \cdot e^{-\frac{\omega_0^2}{2\Delta^2}} \tag{4.1.1}$$

is changing to:

$$E(t) = \left[\cos\left[\omega t\right] + \text{Noise}\right] \cdot e^{-\frac{\omega_0^2}{2\Delta^2}} \tag{4.1.2}$$

The corresponding results are shown in Fig. 4.2 as well as in Fig. 4.3.

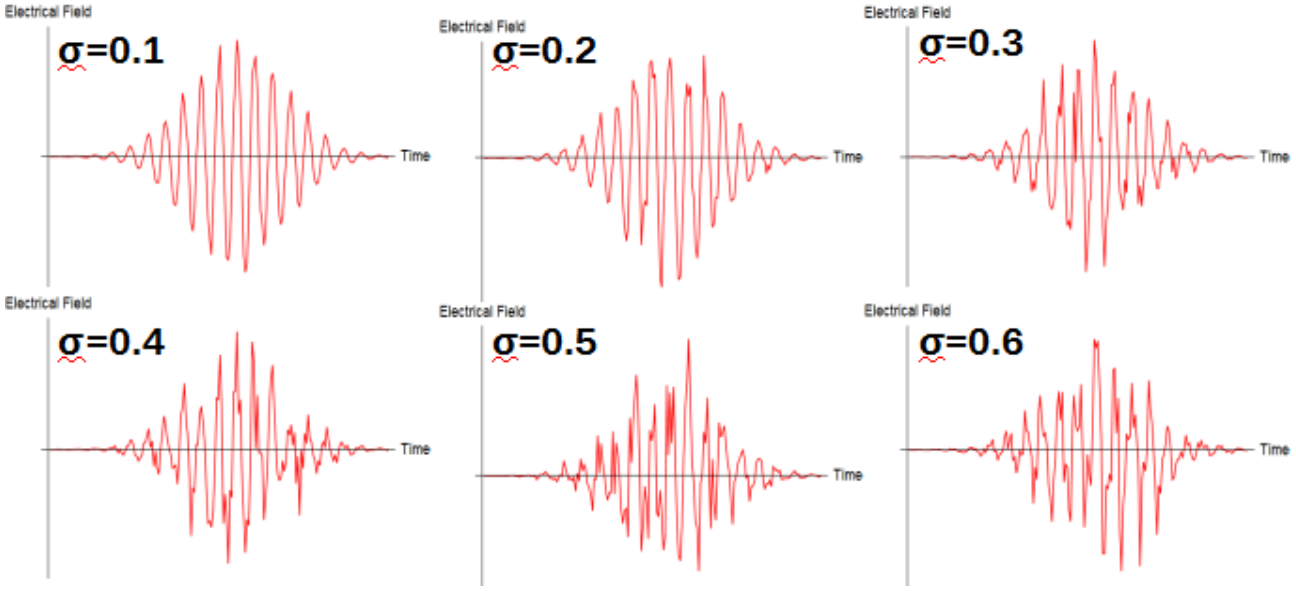

Figure 4.2
A simulated, idealized $p(t)$ pulse with different gaussian white noise added indicated by the standard deviation σ shown in each graph. Notice that just the cosine term was disturbed.

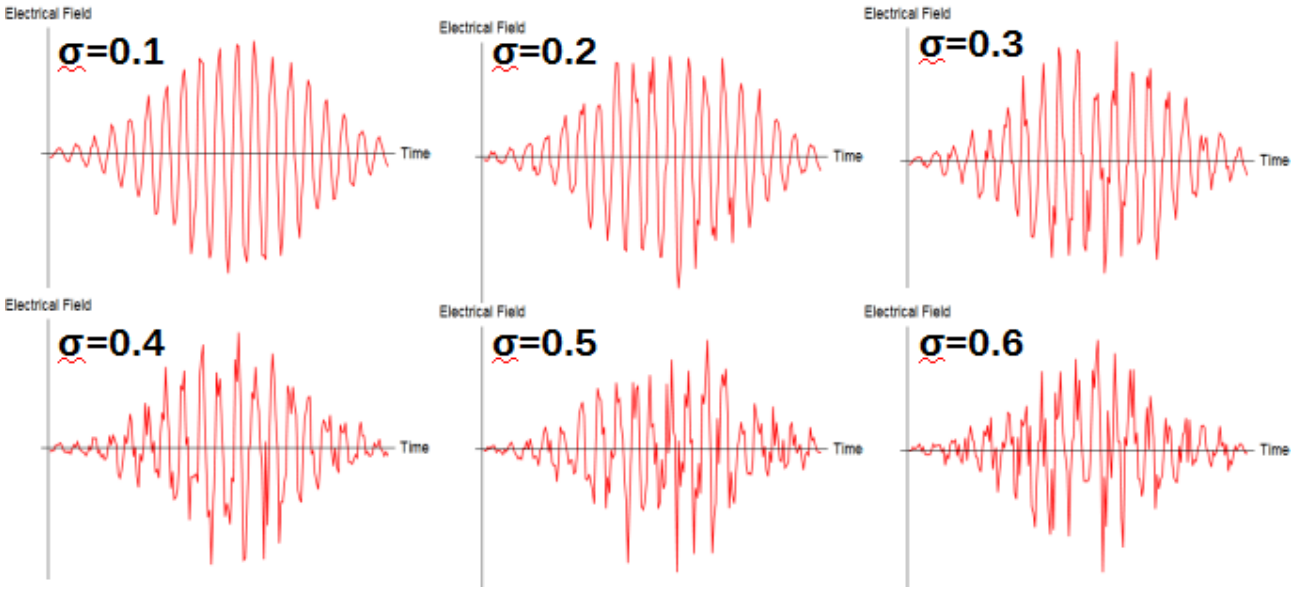

Figure 4.3
A simulated, idealized $g(t)$ pulse with different gaussian white noise added indicated by the standard deviation σ shown in each graph. Notice that just the cosine term was disturbed.

FROG Trace with Gaussian White Noise

In the following paragraph different FROG traces were be disturbed by gaussian noise of different strongness. After that these simulated FROG traces, which were generated out of the $p(t)$– as well as the $g(t)$–pulses, with disturbances are used as an input of the FROG algorithm as the measured FROG trace. From this input the algorithm can determine the correct shaped LASER pulses. In Fig. 4.5 the different simulated FROG traces were shown.

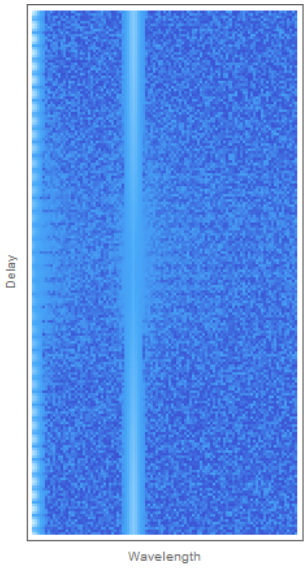

(a) *FROG trace with gaussian white noise added* ($\sigma = 0.1$).

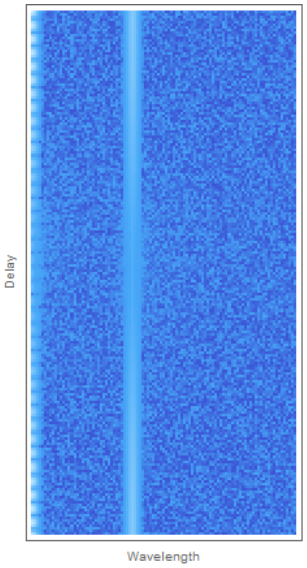

(b) *FROG trace with gaussian white noise added* ($\sigma = 0.3$).

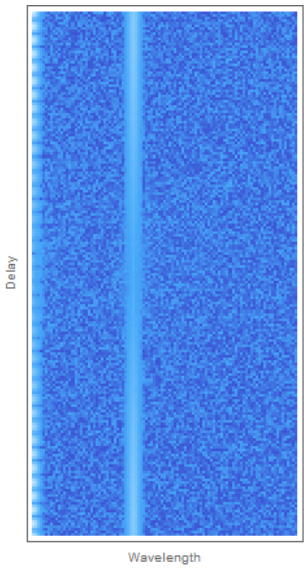

(a) *FROG trace with gaussian white noise added* ($\sigma = 0.5$).

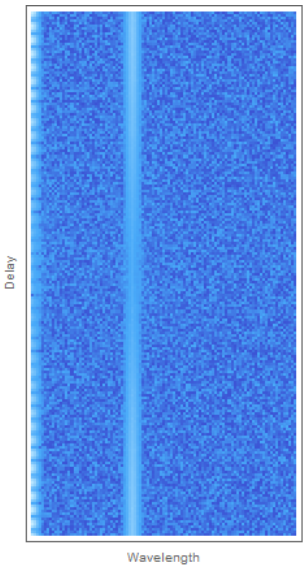

(b) *FROG trace with gaussian white noise added* ($\sigma = 0.6$).

Figure 4.5
Simulated FROG traces by using the pure p– as well as g–pulse overlapping each other. The strongness of the added gaussian white noise is indicated by the standard deviation σ shown in the graphs.

For every simulated and disturbed FROG trace the corresponding pair of ultrashort LASER pulses which have had produced this FROG trace were determined by the algorithm. After that, the known input as well as the determined pulses from the algorithm were analyzed with respect to its magnitude– as well as phase–derivation respectivly. The analyse itself will not be shown in all details, but for better understanding one analysis process will be given as an example.
After the algorithm has determined the correct pulse shape all pulses were normalized. For determining the magnitude as well as the phase a fast Fourier transformation was done. Now the magnitude– as well as the phase–error can be calculated for each of the four pulses. The given initial guess as well as the determined pulses from the algorithm. The magnitude error was determined by calculating the ratio between the input as well as the output. In Tab. 4.2 and Tab. 4.3 the magnitudes as well as the phase errors to the corresponding signal to noise (S/N) ratios are shown. Note that these values were obtained by using pulse length of 200 data points.

Table 4.2
Results of the magnitude error calculation. Notice the small magnitude error by high signal to noise ratio.

	Magnitude Error	
	Noise (S/N)	$\vec{p}(t)$ and $\vec{g}(t)$[%]
p pulse	0	0
	0.1(295.2)	0.09
	0.3(98.4)	0.42
	0.5(60.4)	0.86
	0.6(50.1)	1.11
g pulse	0	0
	0.1(295.2)	0.56
	0.3(98.4)	1.87
	0.5(60.4)	3.60
	0.6(50.1)	4.39

Table 4.3
Results of the phase error calculation. Notice the small phase error by high signal to noise ratio.

	Phase Error	
	Noise (S/N)	$\vec{p}(t)$ and $\vec{g}(t)[Deg]$
p pulse	0	$2.73 \cdot 10^{-22}$
	0.1(295.2)	$3.65 \cdot 10^{-05}$
	0.3(98.4)	$4.26 \cdot 10^{-05}$
	0.5(60.4)	$6.33 \cdot 10^{-02}$
	0.6(50.1)	$2.79 \cdot 10^{-04}$
g pulse	0	0
	0.1(295.2)	$2.41 \cdot 10^{-05}$
	0.3(98.4)	$4.73 \cdot 10^{-05}$
	0.5(60.4)	$6.33 \cdot 10^{-02}$
	0.6(50.1)	$1.82 \cdot 10^{-04}$

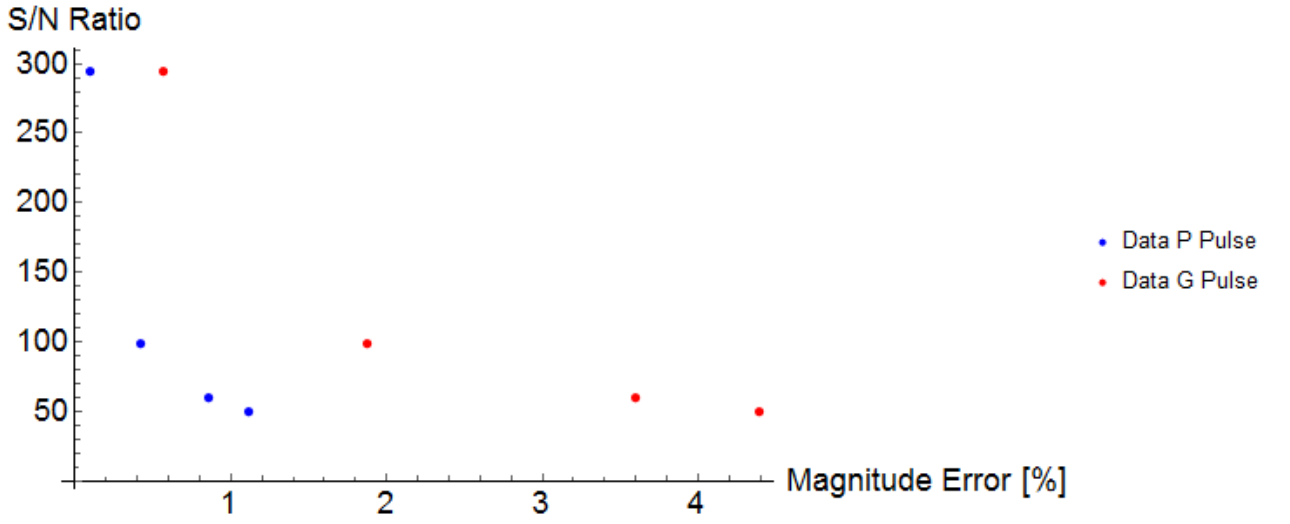

Figure 4.6
For a 200 point long value the corresponding magnitude errors are plotted. The given values can be seen in Tab. 4.2. The blue and red data points representing the $p(t)$ and $g(t)$ pulse respectivley.

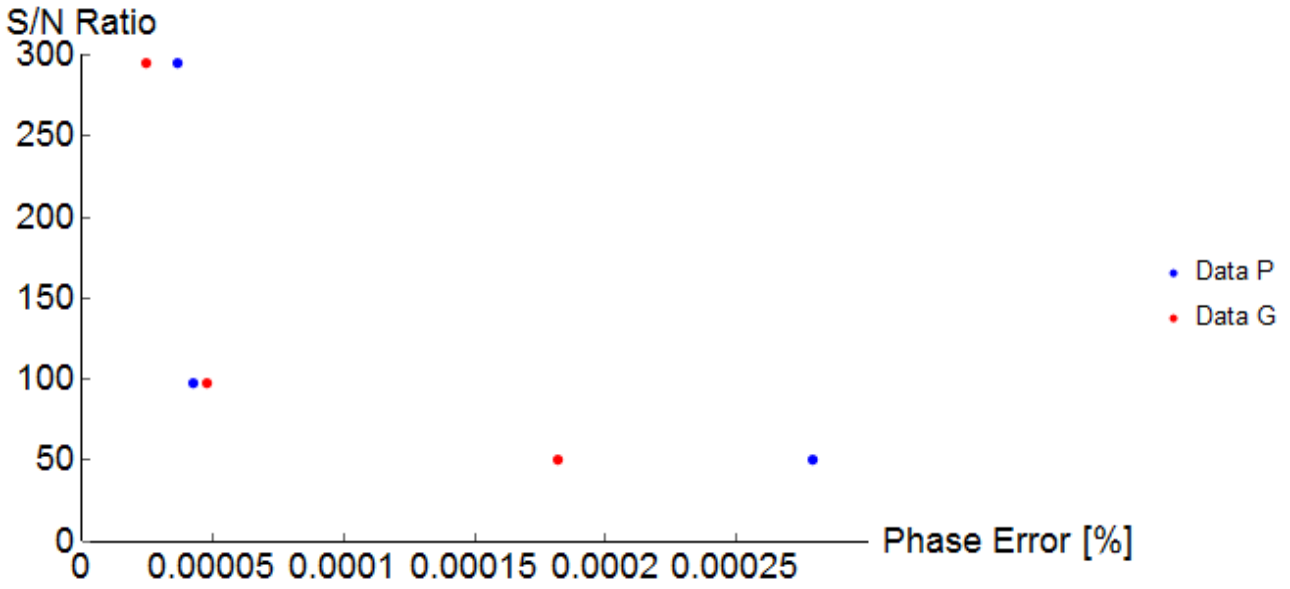

Figure 4.7
For a 200 point long value the corresponding phase errors are plotted. The given values can be seen in Tab. 4.3. The blue and red data points representing the $p(t)$ and $g(t)$ pulse respectivley.

4.1.3 Run Duration Analysis And Accuracy Of The FROG Algorithm

For the run duration analysis a handful different functions were analysed which are used in the FROG algorithm and have a great impact on the run duration of this algorithm.
These functions are:

- the fast Fourier transformation (FFT)
- the inverse fast Fourier transoformation (IFFT)
- the single value decomposition (SVD)
- the power method as an replacement for the SVD

For the test itself a test algorithm was developed. This test algorithm was developed with LabVIEW™ 2017, 64–bit version[1]. In Fig. 4.8 the source code of the test function is shown. Notice the increasing matrix size in every loop iteration as well as the "Calc FFT" function which was replaced gradual by the other above mentioned functions.

Furthermore, take attention that all mentioned function were implemented as a multicore function if possible. These functions using all existing cores of the used computer which decreases the calculation time in total. Moreover, this was not additional programmed. Luckily, LabVIEW™ has some specific functions already written for multicore purposes[2]. Therefore, the actually programmer saves time by using them. The used multicore functions were the inverse as well as the fast Fourier transformation, the single value decomposition and different matrix functions like calculation of the outer product and matrix multiplication.

[1] The test function was build on a Dell computer with an Intel Core i5 processor with 3.30 GHz, 8 GB RAM, with the motherboard 00V62H by using Windows 7 Enterprise edition (64–bit version)

[2] These functions could be installed additionally by using the so–called "VI Package Manager". Just search for "Multicore Analysis and Sparse Matrix Toolkit"

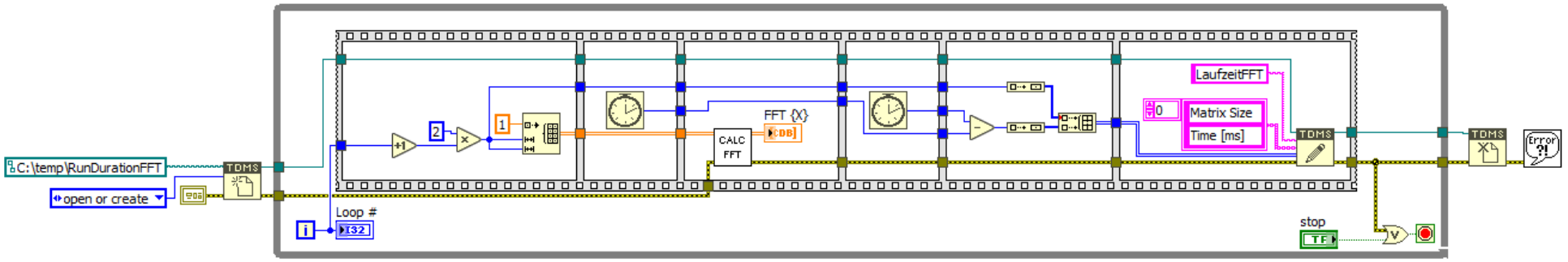

Figure 4.8

Source code of the developed function for the run duration analysis for all used functions in the FROG algorithm. Note that the function "Calc FFT" is given as an example. Further, for all functions an increasing matrix was used with value one for all elements.

After all functions were tested the different matrix sizes as well as the time were plotted. This is shown in Fig. 4.9. Here the red curves represents the data size in dependence of time and the green curves are the fit. Notice that all four of them has a quadratic behaviour. Therefore the time needed to calculate the corresponding values goes quadratic with the size of the matrix for all functions. Especially, the FFT, IFFT, SVD as well as the PM. Further, which is obviously is the unstatic behaviour of the red curves. This can be described by the internal computer "problems" like memory allocation, storing the data as well as the normal jitter which occurs due to internal Microsoft Windows^{TM} processes.

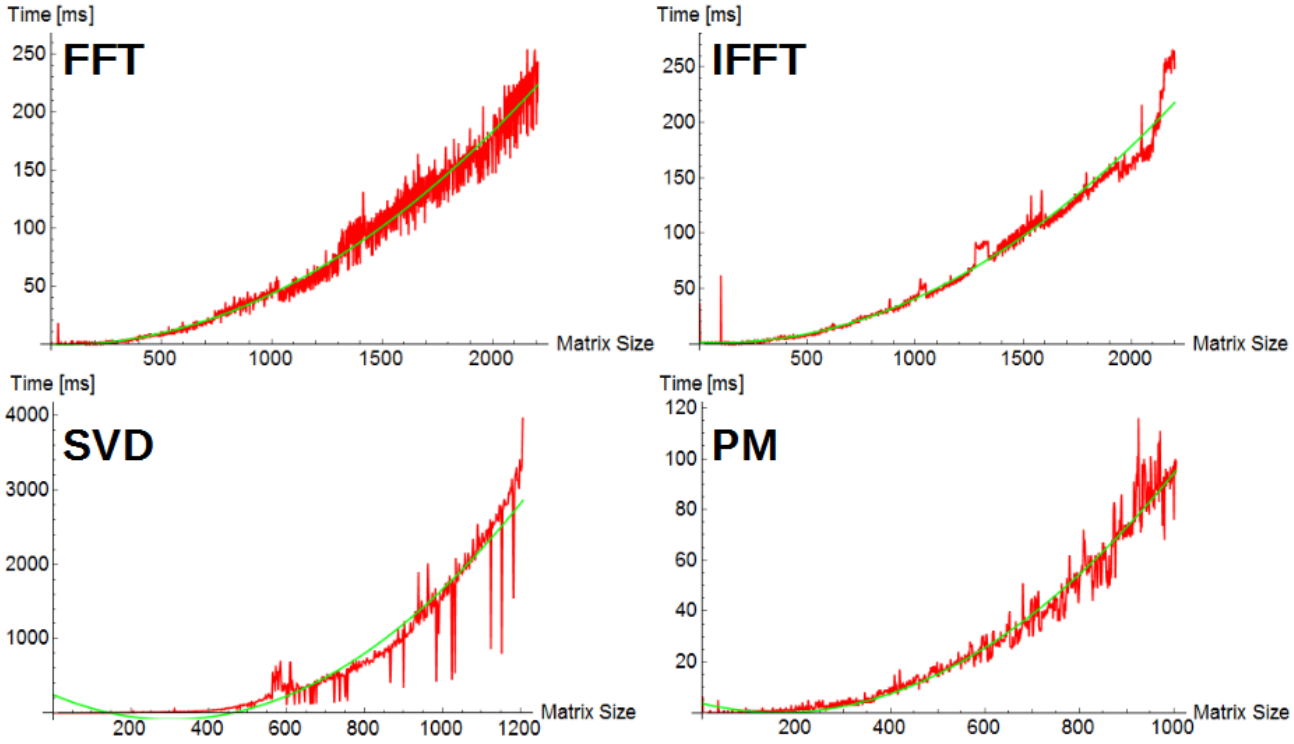

Figure 4.9

*Time behaviour in dependence of the matrix size of the fast Fourier transformation (**FFT**), the inverse fast Fourier transformation (**IFFT**), the single value decomposition (**SVD**) as well as the Power Method (**PM**). Red curves representing the data points and the green curves are the fit. Notice the quadratic behaviour of the form $f(x) = ax^2 + bx + c$ of all four functions which is represented by the green curves.*

4.2 Conclusion

a) Reliability of the PCGP–algorithm

The implemented PCGP–algorithm was testet with different types of idealized gaussian pulses. On the one hand the pure non–disturbed gaussian pulses were put into the algorithm and on the other hand also idealized gaussian disturbed pulses were used. Whereas the disturbances are just added gaussian white noise. Furthermore, simulated FROG traces with and without disturbances were investigated ...

b) Run Duration Analysis

The self established application for testing the run duration of the four main functions provided information about the temporal behaviour in dependence of the used input size. All of the functions, except the power method, receive a matrix as input. The analysing procedure achieved a quadratic temporal behaviour of the form $f(x) = ax^2 + bx + c$ where x is the size of the quadratic matrix (see Fig. 4.9). Therefore the slowest part of the whole algorithm – the so–called bottle–neck – are these four functions, namley the inverse fast Fourier transformation, the fast Fourier transformation, the single value decomposition as well as the power method.

Chapter 5

Experimental Setup and Functioning

In the following chapter the experimental setup will be described. This setup was build for determining and investigation of the shape and phase of ultra short infrared LASER pulses. These pulses can be investigated as a pure pulse but also after they passed some media. Especially fluids can be interesting due to the fact, that they are widespread in the environment.
These gases can be i. e. methane or carbon dioxid as well as water vapor. All of these mentioned fluids have specific absorption bands which can have some influence in the shape and phase if the infrared LASER pulse is traveling through it. In Appendix A there are absorption spectra in dependence of the wavenumber shown for carbon dioxide, methane and water respectively. However, due to technical reasons this will not be investigated in this thesis. In the next chapter a description of the SFG–FROG setup will be given.

5.1 The FROG–Device

In the last sections the basic concept of a FROG–system as well as the powerfullness of the implemented PCGP–algorithm in LabVIEW^{TM} were described. Up to now there are a huge amount of different systems available to characterize ultra short LASER pulses. These system are i . e . the IFROG, XFROG or the GRENOUILLE respectively. An extract of commercially available systems are given in Appendix C with a short description. In comparison with all the other FROG systems the SFG–FROG system is easy to build and has a low costs profile due to the fact that no expensive IR spectrometer or camera is used. This is due to the conversion from 800 nm LASER beam and the IR LASER beam to the visible SFG beam. This SFG–FROG is the only one which transfers the IR problem into the visible region. In the following the different parts of the SFG–FROG setup will be described

5.2 The SFG–FROG–Setup

As mentioned in the previous chapters the SFG–FROG setup was build to be able to investigate ultrafast LASER pulses. Especially, its shape which corresponds to its phase as well as its magnitude.
The SFG–FROG system consists of six different parts which has some influence on the incident LASER beams. In Fig. 5.1 a scheme of the builded FROG system is shown. Here the s–polarized 800 nm LASER pulse is indicated as the green arrows as well as the red arrows are representing the infrared LASER pulses.

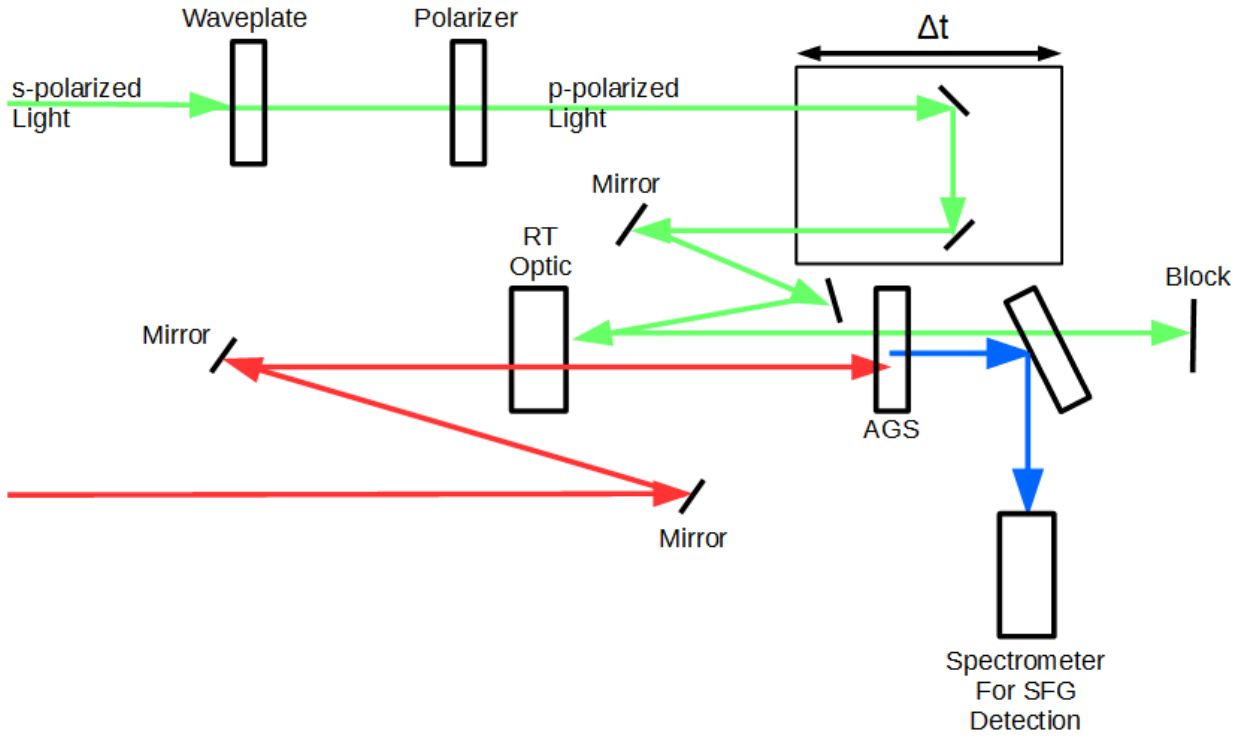

Figure 5.1
Schematic setup of a SFG–FROG. The p–polarized 800 nm (green) and s–polarized IR (red) LASER beam generating a SFG (blue) beam by overlapping in space and time in a silver thiogallate crystal (AGS). Moreover, a special optic (RT optics) was mounted to achieve a collinear beam propagation.

As mentioned and shown in the above scheme the used 800 nm LASER beam is s–polarized. Due to the properties of the silver–thiogallate crystal this polarization had to be changed. For that a waveplate was used. This optical item rotates the wave about a half wavelength. Therefore this kind of waveplate is called: $\lambda/2$–waveplate and after this item the resulted wave is p–polarized. However, due to i. e. misalignment this rotation can affect not all parts of the s–polarized wave beam. For overcoming this task a polarizer was used. This polarizer is a 90/10–polarizer. This means that 90% of the upcoming s–polarized wave beam will be reflected if the corresponding optical item is mounted in an angle of 45° to the beam path and just the p–polarized beam goes through. After that the corresponding p–polarized 800 nm LASER beam is reflected by gold mirrors to the RT–Optic[1].
Further, a computer controlled delay stage was used to generate a time–shift between the 800 nm and IR–LASER–pulse. This is necessary to achieve a spatial as well as temporal overlay between both LASER beams in the crystal. This fact is important because otherwise no SFG can be produced.

[1] RT stands here for "Reflective–Transparent–Optic"

One of the most important items is the "RT–Optic"'. This item is reflective for 800 nm and transparent for infrared radiation[2] and was used to obtain a collinear LASER beam propagation of both LASER beams towards the silver–thiogallate crystal.
Moreover, for investigation reasons the wavelength of the infrared LASER beam will be change its value during the experiment in the range of: $(3\mu m \leq \lambda \leq 12\mu m)$. After both beams pass the same path they are going to overlap spatial as well as temporal in the silver–thiogallate crystal. Here the SFG–beam will be produced which will go into a computer connected spectrometer[3]. This generation is a second order process. In order to achieve such second order process the used crystal has to fulfill specific properties.
On the one hand the crystal has to be a nonlinear one with a non–inversion symmetry. It has to be transparent in the range of $(0.6\,\mu m \leq \lambda \leq 12\,\mu m)$. On the other hand the crystal has to fulfill a so–called phase–matching condition which results into a specific wavelength dependent angle. This angle has to be calculated. For a detailed determination of the phase–matching anlge please take a look into the Appendix B

[2] Notice that this optical item was created especially for this SFG–FROG setup. The corresponding coatings are not known due to the concealment policy of the company which it had made.
[3] Here a spectrometer from the company Ocean Optics was used. Especially, the device HR2000ES+.

Chapter 6

The First Test, Evaluation And Discussion

6.1 The FROG In Action

In the previous chapters we took a look into the theory of LASERs, how a FROG device is working in general as well as how we can determine the shape and phase of an ultra short LASER pulse. All information keeping in mind we are now able to do the real measurement. The first real FROG–trace and therefore the proof of principle was done by Dr. Yujin Tong and me on May 18th, 2018. Here the HR2000+ spectrometer from the company Ocean Optics which has a detection range of 490 nm up to 1200 nm was used.
However, the used crystal was a lithium niobate one instead of the silver thiogallate due to calibration reasons.
In the following the test measurements as well as verifying the FROG application which was written will be handled. Further, the different FROG–traces with different wavelengths by using the silver–thiogallate will be discussed and remarks what the experimentalist has to take care about to obtain good results will be mentioned.

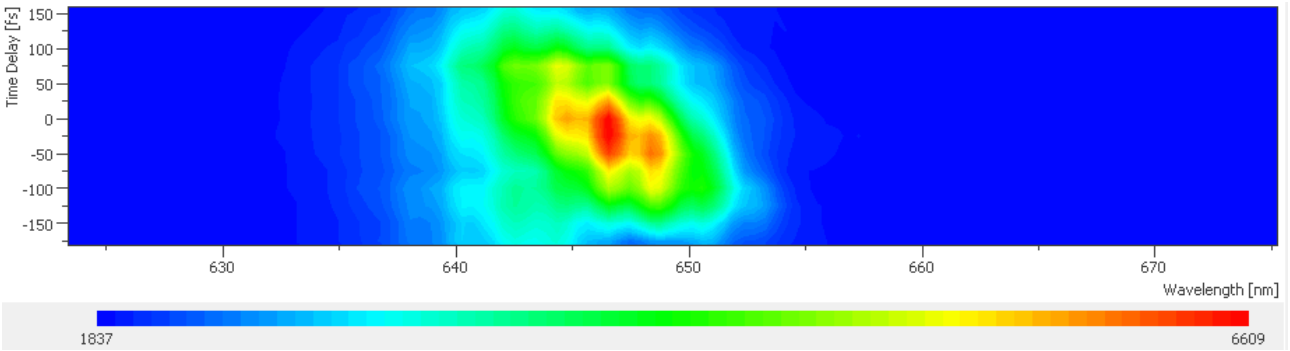

Figure 6.1
The shown FROG–trace which was obtained by overlapping a 800 nm and a 4000 nm infrared pulse in a silver–thiogallate crystal. Notice the three time maximum intensity distribution in the middle of the FROG–trace. These structure happens due to spatial shift of the used LASER.

6.2 The Proof Of Principle

After build up the corresponding SFG–FROG setup a first test was done. This test was necessary to be sure, that the SFG production is possible with collinear LASER beams. Further, instead of using a silver–thiogallate crystal a lithium niobate crystal was used. The first result is shown in Fig. 6.2.

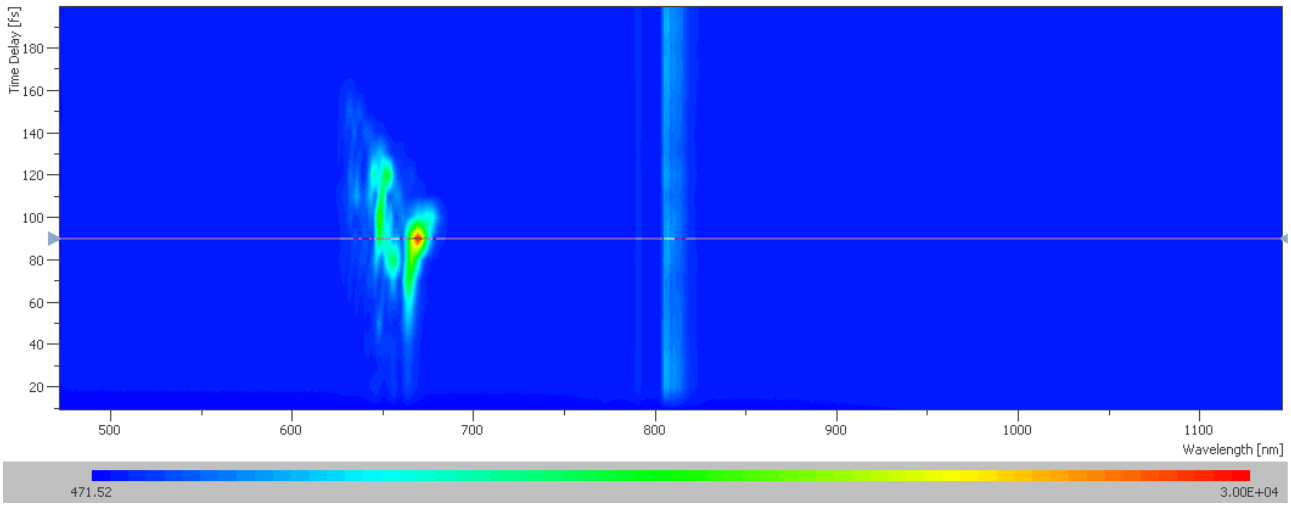

Figure 6.2
First measured FROG trace which is located on the left side of this picture. On the right side you see some reflection of the used 800 *nm LASER beam. Due to the fact that all beams are collinear to each other a reflective optic was used to separate them from each other. Here an optic which was* 90 *% transmittable for the* 800 *nm LASER beam was used. The used crystal to generate SFG was a lithium niobate crystal.*

The reason for using the lithium niobate crystal first was on the one hand the lithium niobate crystal is off bigger size and therefore the alignment was much easier. On the other hand it was not known how strong the SFG–signal of the silver–thiogallate crystal would be. The SFG–signal of a lithium niobate crystal is quite strong and can be easily seen by eye.
Moreover, after the SFG–signal was generated just the lithium niobat crystal has to be replaced by the silver–thiogallate crystal. Due to the difference in their size the corresponding temporal and spatial overlap is not valid anymore. For that, the delay stage will used to overcome these difference.
Note that due to a bug in the algorithm the time axis has a wrong scale in Fig. 6.2. Here the time zero point is at 90 fs indicated by the purple line. Further, a not proper alignment produced the second FROG–trace on the left side of the main one (the main one has a higher intensity in the middle). Furthermore, some artefact at 800 nm is visible. This is due to a 90/10% reflective optic which was used to get rid of the main part of the 800 nm LASER beam after the SFG–signal was generated. Remember that all LASER beams are travelling collinear.

6.2.1 FROG Traces with Lithium Niobate

After the first successful proof of principle further FROG–traces by using the lithium niobate crystal were measured. In Fig. 6.3 and Fig. 6.4 two measured FROG–traces are shown. However, due to the properties of the lithium niobate crystal it was not possible to go farther refering the wavelength. The transmittance of wavelengths between 1μm and 5μ m are 60% but at 6μm this transmittance decreased to zero.
By investigating the corresponding FROG–traces it is obvious that the intensity distribution has its maximum in the center of the signal. This makes totally sense due to the fact that one pulse is scanned over the other and reaches its maximum at zero overlap. This is happen by a time delay of 45 fs. Note that the time scale is not quite correct. The zero point, where the overlapping has its maximum should be at, like just mentioned, at 45 fs all numbers greater than 45 fs should be negative and all numbers less than 45 fs should be positive referring the zero time scale. The negative times representing a later incoming whereas the positive indicates an early incoming of the corresponding LASER pulse. This is caused regretly due to the previous mentioned bug in the algorithm.

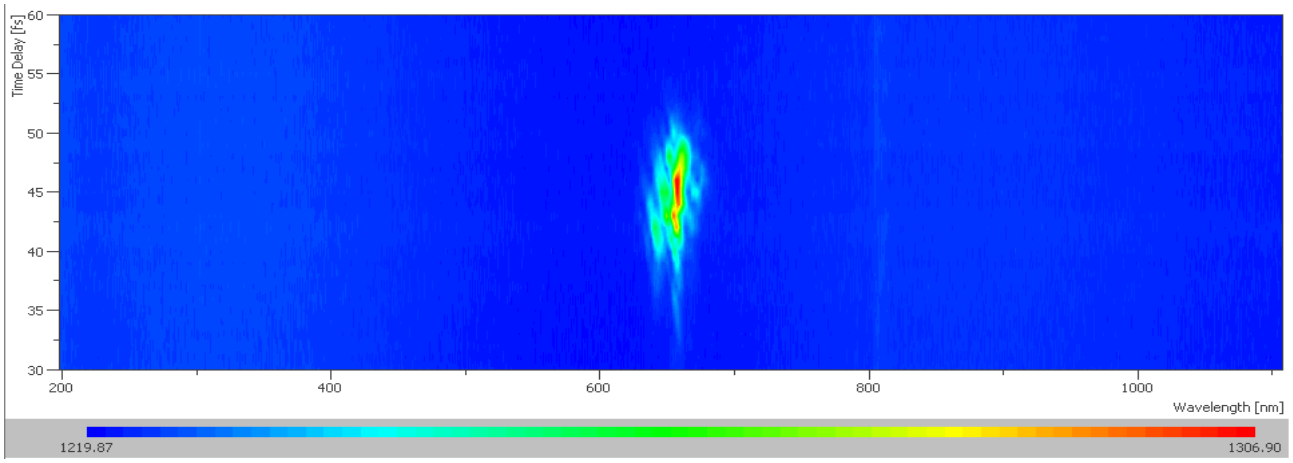

Figure 6.3
A measured FROG–trace at 4000 *nm by using a lithium niobat crystal. For a better result* 1000 *measurement cycles were averaged.*

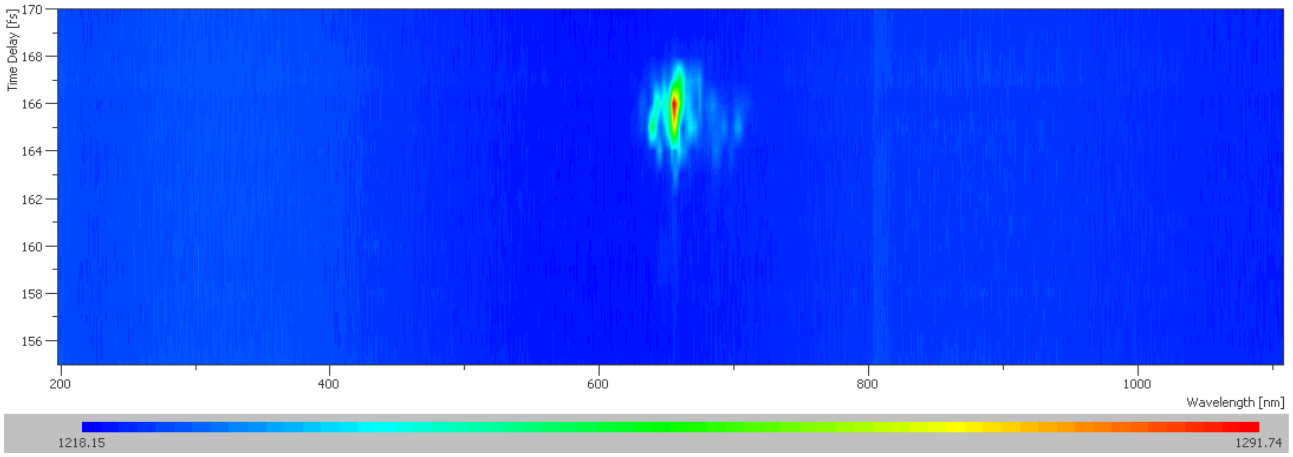

Figure 6.4
A measured FROG–trace at 5000 *nm by using a lithium niobat crystal. For a better result* 1000 *measurement cycles were averaged.*

Acknowledgment

At the end of this thesis I want to thank everybody which had some influence on me, my writing, working as well as thinking about the one or other task which I had to solve to achieve enough information, knowledge and encouragement to finish these thesis.
At first, I want to thank Prof. Martin Wolf for the possibility to operate at the Fritz–Haber Institute of the Max Planck Society as well as his dedication to encourage me to finish this important mile stone in my life.
I want to thank Dr. H. Kirsch, without his encouragement I had maybe never the possibility to work at the Fritz–Haber–Institut. I also like to thank my good friend and colleague Albrecht Ropers for his great expertise in quite all computer science questions which he had shared with me and still does, his special way to teach me also a huge amount of different other subjects and patience by teaching me in general. His wise words and notes brought me the right ideas. Further I want to thank Marcel Krenz for also teaching me a bunch of things but also for introducing me LabVIEW™. A programming language which I lost my heart to.
I want to thank Selene Mor, Julius Heitz and Dr. Lukas Z. Braun, Angelika Demling and Dr. C. Schewe for their intense, fruitful discussions referring different subjects during my writing. Manuel Krüger for his clear and supporting words during my time of demotivation and bringing me back track again. Petra Hering for spending a huge time listen to me and my issues. Also I would like to thank Prof. T. Kampfrath and S. Kubala who brought always joy in my life which motivated myself to go on.
Last but not least I want to thank my family for the strong support and their patience during my studies, their clear words and suggestions referring my work and bringing my thoughts into the right directions.
Without all of you this thesis could had never be written!

Thank you!

Appendix A

Transmittance Infrared Spectra

In the following different infrared absorption spectra will be shown. They show different dips in its spectra each. These dips show the absorption at a specific wavelength given in units of reciprocal centimeters[1]: cm^{-1}, the so–called wavenumber or repetency. Take attention to the unit. In this thesis the SI–units[2] will be used. The following equation can be used to calculate the different wavelengths to each other

$$\lambda[nm] = \frac{10^7}{\lambda[cm]} \tag{A.1.1}$$

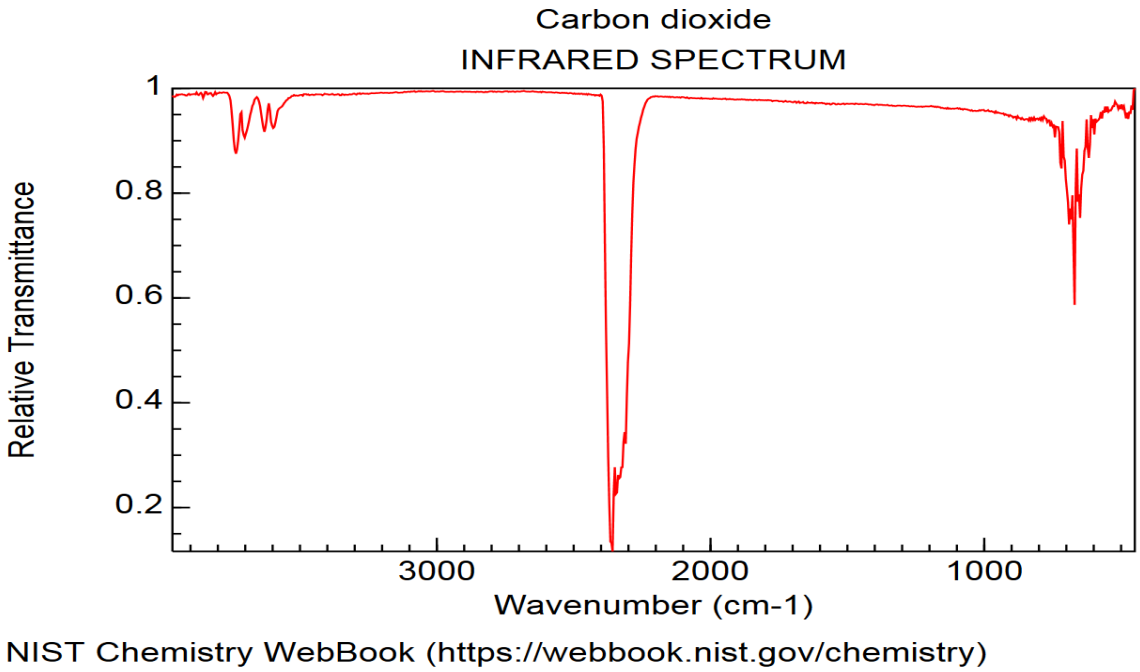

Figure A.1
The infrared absorption spectrum of carbon dioxid. Notice the main absorption dips around $650cm^{-1} = 15385\,nm$, $2350cm^{-1} = 4300\,nm$ *as well as* $3700cm^{-1} = 2700\,nm$

[1] This unit cannot be found in old books. Instead of this the unit "kayser" was used. They was named after Heinrich G. J. Kayser, a german physicist. In the SI-units is $1\,\text{kayser} = 100m^{-1}$

[2] SI is an abbreviation and stands for système international d'unité . This is french and means international system of units. This system based on seven units in total was introduced in 1960 to achieve consistency in the building of units. Every unit can be generated by using these basic seven units.

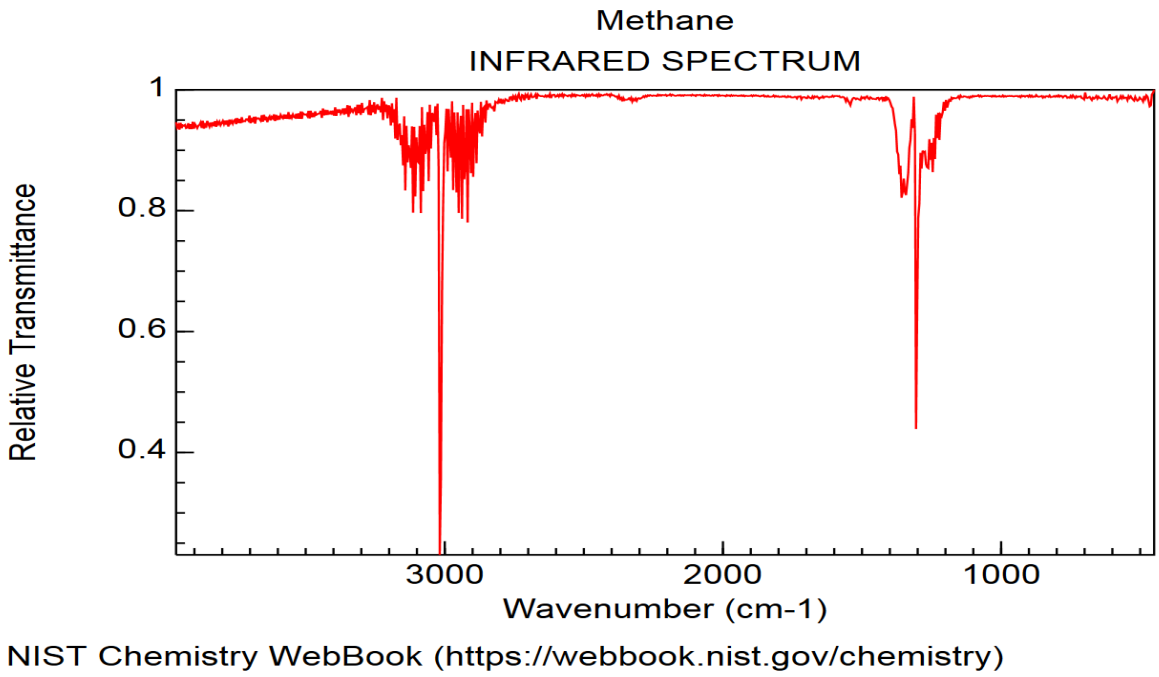

Figure A.2
The infrared absorption spectrum of methane. Notice the main absorption dips around $1300cm^{-1} = 7692\,nm$ *and* $3000cm^{-1} = 3300\,nm$

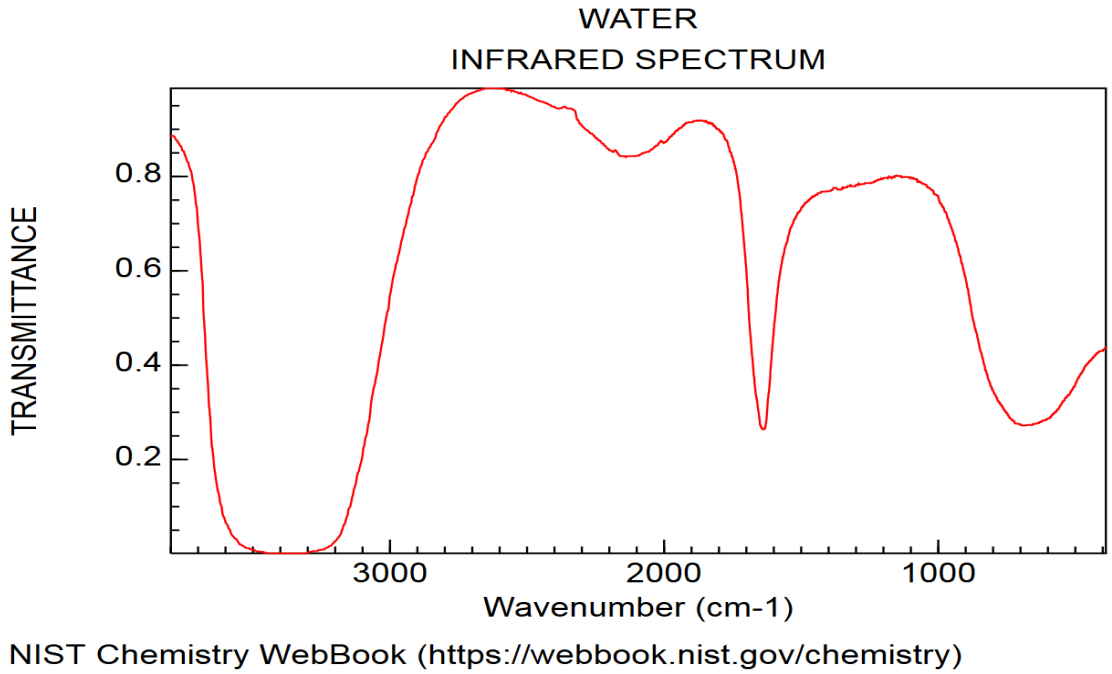

Figure A.3
The infrared absorption spectrum of water. Notice the main absorption dips around $700cm^{-1} = 14286\,nm$, $1600cm^{-1} = 6250\,nm$, $2100cm^{-1} = 4762\,nm$ *as well as* $3400cm^{-1} = 2940\,nm$

Appendix B

Derivation Of The Phase Matching Angle

For generating a SFG–beam it is necessary to understand when and why this second order process is happening. For that a closer look to the Maxwell equations is taken first. These can be defined in dual tensor form like [6]:

$$F^{\mu\nu} = \frac{1}{c}\begin{pmatrix} 0 & E_x & E_y & E_z \\ -E_x & 0 & cB_z & -cB_y \\ -E_y & -cB_z & 0 & cB_x \\ -E_z & B_y & -cB_x & 0 \end{pmatrix} \tag{B.1.1}$$

$$G^{\mu\nu} = \frac{1}{c}\begin{pmatrix} 0 & cB_x & cB_y & cB_z \\ -cB_x & 0 & -E_z & E_y \\ -cB_y & E_z & 0 & -E_x \\ -cB_z & -Ey & E_x & 0 \end{pmatrix} \tag{B.1.2}$$

Whereby c is the speed of light, E_i and B_i are the i–th component of the electrical field as well as the magnetic field of the electromagnetic wave respectivly. Notice, that this is a compact form to write all four Maxwell equations with respect to the space time.
By using these equations with $\mu = 0$ one receives the first Maxwell equation:

$$\sum_{\nu=0}^{3} \frac{\partial F^{\mu}}{\partial x^{\nu}} = \mu_0 J^0 \tag{B.1.3}$$

$$\mu_0 = 0: \quad \mu_0 J_0 = \mu_0 c\rho \tag{B.1.4}$$

$$= \frac{1}{c}\left(\frac{\partial E_x}{\partial x} + \frac{\partial E_y}{\partial y} + \frac{\partial E_z}{\partial z}\right) \tag{B.1.5}$$

$$= \frac{1}{c}(\nabla \cdot \vec{E}) \tag{B.1.6}$$

$$\Rightarrow \nabla \cdot \vec{E} = \frac{1}{\epsilon_0}\rho \quad \text{with } c = \frac{1}{\sqrt{\mu_0 \cdot \epsilon_0}} \tag{B.1.7}$$

By using $\mu_0 = 1, 2, 3$ one achieves the fourth Maxwell equation:

$$\mu_0 = 1: \quad \mu_0 J_x = (-c^{-2}\frac{\partial \vec{E}}{\partial t} + \nabla \times \vec{B})_x \tag{B.1.8}$$

$$\mu_0 = 2: \quad \mu_0 J_y = (-c^{-2}\frac{\partial \vec{E}}{\partial t} + \nabla \times \vec{B})_y \tag{B.1.9}$$

$$\mu_0 = 3: \quad \mu_0 J_z = (-c^{-2}\frac{\partial \vec{E}}{\partial t} + \nabla \times \vec{B})_z \tag{B.1.10}$$

$$\Rightarrow \mu_0 \vec{J} = -c^{-2}\frac{\partial \vec{E}}{\partial t} + \nabla \times \vec{B} \tag{B.1.11}$$

$$\Rightarrow \nabla \times \vec{B} = \frac{1}{c^2}\frac{\partial \vec{E}}{\partial t} + \mu_0 \vec{J} \tag{B.1.12}$$

Moreover, to receive the other two missing Maxwell equations one has to use Equ. B.1.2. Also here by choosing $\mu = 0$ follows:

$$\sum_{\nu=0}^{3} \frac{\partial G^\mu}{\partial x^\nu} = 0 \tag{B.1.13}$$

$$= \frac{1}{c}\left(c\frac{\partial B_x}{\partial x^1} + c\frac{\partial B_y}{\partial x^2} + c\frac{\partial B_z}{\partial x^3}\right) \tag{B.1.14}$$

$$= \nabla \cdot \vec{B} \tag{B.1.15}$$

$$\Rightarrow \nabla \cdot \vec{B} = 0 \tag{B.1.16}$$

By using this equation with $\mu = 1, 2, 3$ one receives:

$$\sum_{\nu=0}^{3} \frac{\partial G^\mu}{\partial x^\nu} = 0 \tag{B.1.17}$$

$$\mu_0 = 1: \quad 0 = \frac{1}{c}\left(-c\frac{\partial B_x}{\partial x^0} - \frac{\partial E_z}{\partial x^2} + \frac{\partial E_y}{\partial x^3}\right) \tag{B.1.18}$$

$$= (\nabla \times \vec{E} + \frac{\partial B}{\partial t})_x \tag{B.1.19}$$

$$\mu_0 = 2: \quad 0 = \frac{1}{c}\left(-c\frac{\partial B_y}{\partial x^0} - \frac{\partial E_x}{\partial x^2} + \frac{\partial E_z}{\partial x^3}\right) \tag{B.1.20}$$

$$= (\nabla \times \vec{E} + \frac{\partial B}{\partial t})_y \tag{B.1.21}$$

$$\mu_0 = 3: \quad 0 = \frac{1}{c}\left(-c\frac{\partial B_z}{\partial x^0} - \frac{\partial E_y}{\partial x^2} + \frac{\partial E_x}{\partial x^3}\right) \tag{B.1.22}$$

$$= (\nabla \times \vec{E} + \frac{\partial B}{\partial t})_z \tag{B.1.23}$$

$$\Rightarrow 0 = \nabla \times \vec{E} + \frac{\partial \vec{B}}{\partial t} \tag{B.1.24}$$

$$\Rightarrow \nabla \times \vec{E} = -\frac{\partial \vec{B}}{\partial t} \tag{B.1.25}$$

In the latter the four Maxwell equations were build out of the tensor form. However, these equations are valid for vacuum and will change due to the fact that we are dealing with matter. Therfore, the whole Maxwell equations will change to[1]:

$$\nabla \cdot \vec{D} = \rho_f \quad \text{with } \vec{D} = \epsilon_0 \vec{E} + \vec{P} = \epsilon_0 \cdot \epsilon_r \cdot \vec{E} \tag{B.1.26}$$

$$\nabla \cdot \vec{B} = 0 \tag{B.1.27}$$

$$\nabla \times \vec{E} = -\frac{\partial}{\partial t}\vec{B} \tag{B.1.28}$$

$$\nabla \times \vec{H} = \vec{J}_f + \frac{\partial}{\partial t}\vec{D} \tag{B.1.29}$$

By assuming a non–magnetizable ($\vec{M} = \vec{0}$), polarisable but no having free charges ($\rho_f = 0$) as well as no free current available ($\vec{J}_f = 0$) these Maxwell equations will reduce to:

$$\nabla \cdot \vec{D} = 0 \tag{B.1.30}$$

$$\nabla \cdot \vec{B} = 0 \tag{B.1.31}$$

$$\nabla \times \vec{E} = -\frac{\partial}{\partial t}\vec{B} \tag{B.1.32}$$

$$\nabla \times \vec{H} = \frac{\partial}{\partial t}\vec{D} \tag{B.1.33}$$

Furthermore I have to mention that we are dealing with a nonlinear medium. For that the scalars like the relative permittivity ϵ_r of the matter will change to a direction dependent tensor which is also depended of the frequency. So the corresponding displacement equation will change to:

$$\vec{D} = \epsilon_0 \cdot \vec{E} + \vec{P} = \epsilon_0 \cdot \epsilon^{ij}(\omega) \cdot \vec{E} \quad \text{with} \tag{B.1.34}$$

$$\vec{P} = \epsilon_0 \cdot \chi_e(\omega) \cdot \vec{E} \cdot \left(\underbrace{1}_{\text{linear part}} + \underbrace{\chi_e(\omega)\vec{E} + \chi_e^2(\omega)\vec{E}^2 \ldots}_{\text{nonlinear part}} \right) \tag{B.1.35}$$

Notice that the tensor of relative permittivity is a hermitian and therefore a symmetric tensor. A nice property of all hermitian matrices is that all are diagonalisable. Furthermore, due to low absorption they are real and have the following form:

$$\epsilon_r(\omega) = \begin{pmatrix} \epsilon_{xx}(\omega) & 0 & 0 \\ 0 & \epsilon_{yy}(\omega) & 0 \\ 0 & 0 & \epsilon_{zz}(\omega) \end{pmatrix} = \begin{pmatrix} n_{xx}^2 & 0 & 0 \\ 0 & n_{yy}^2 & 0 \\ 0 & 0 & n_{zz}^2 \end{pmatrix} \quad \text{with} \quad n = \sqrt{\mu_r \epsilon_r(\omega)} \tag{B.1.36}$$

Moreover, I deal with an negative uniaxial crystal. It is known that for such kind of crystals the refractive index is:

$$n_x = n_y = n_o \quad \text{the ordinary wave path} \tag{B.1.37}$$

$$n_z = n_e \quad \text{the extraordinary wave path} \tag{B.1.38}$$

Due to the fact that I am using a uniaxial, birefringence crystal one can use the Fresnel–equation:

$$0 = \sum_{i=1}^{3} \frac{\vec{e}_i^2}{\frac{1}{n_i^2} - \frac{1}{n^2}} \tag{B.1.39}$$

[1] For a detail derivation from the Maxwell equations in vacuum to the Maxwell equations in matter please take a look to [6]

For determining the specific phase matching angle one has to consider the electric energy density:

$$w_e = \frac{1}{2} \cdot \vec{E} \cdot \vec{D} \quad \text{with } \vec{E} = \frac{\vec{D}}{\epsilon_r \epsilon_0} = \frac{\vec{D}}{n^2 \epsilon_0} \tag{B.1.40}$$

$$= \frac{1}{2 \cdot \epsilon_0} \cdot \left(\frac{D_x^2}{n_x^2} + \frac{D_y^2}{n_y^2} + \frac{D_z^2}{n_z^2} \right) \tag{B.1.41}$$

$$\Rightarrow 1 = \frac{d_x^2}{n_x^2} + \frac{d_y^2}{n_y^2} + \frac{d_z^2}{n_z^2} \quad \text{with} \quad \vec{d} = \frac{\vec{D}}{\sqrt{2\epsilon_0 \cdot w_e}} \tag{B.1.42}$$

The last equation is called index ellipsoidal equation and defines – like the name suggest – an ellipsoid. By assuming that the corresponding $\vec{D}_i$ are equal with the axis and using the spherical coordinates of the form:

$$\begin{pmatrix} x \\ y \\ z \end{pmatrix} = r \cdot \begin{pmatrix} \sin[\theta] \cdot \cos[\phi] \\ \sin[\theta] \sin[\phi] \\ \cos[\theta] \end{pmatrix} \tag{B.1.43}$$

After plugging in everything give an index ellipsoid of the form (assuming $1/r^2 = 1/n(\theta,\omega)$):

$$\frac{1}{n^2(\theta,\omega)} = \frac{\cos^2[\theta]}{n_o^2} + \frac{\sin^2[\theta]}{n_e^2} \tag{B.1.44}$$

Please keep in mind that fully ellipsoidal equation is: $1 = x^2/n_x^2 + y^2/n_y^2 + z^2/n_z^2$. This equation was modified by using the spherical coordinates as well as the assumption that $\phi = 0$.
By using the Sellmeiers equation one can calculate the corresponding refractive index of the ordinary (n_o) as well as the extraordinary (n_e) wave. Notice that the following equations are valid for ($0.54\mu m < \lambda < 12.9\mu m$) only but they representing a good approximation [15]:

$$n_o^2 = 5.79419 + \frac{0.23114}{\lambda^2 - 0.06882} - \frac{2.4534 \cdot \lambda^2}{10^3} + \frac{3.1814 \cdot \lambda^4}{10^7} - \frac{9.7051 \cdot \lambda^6}{10^9} \tag{B.1.45}$$

$$n_e^2 = 5.54120 + \frac{0.22041}{\lambda^2 - 0.09824} - \frac{2.5240 \cdot \lambda^2}{10^3} + \frac{3.6214 \cdot \lambda^4}{10^7} - \frac{8.3605 \cdot \lambda^6}{10^9} \tag{B.1.46}$$

Furthermore the following phase matching equations has to be fullfilled:

$$\omega_1 + \omega_2 = \omega_3 \tag{B.1.47}$$

$$\omega_1 \cdot n(\omega_1) + \omega_2 \cdot n(\omega_2) = \omega_3 \cdot n(\omega_3) \tag{B.1.48}$$

Moreover we are dealing with a type II process (e–o–e)[2]. Therefore Equ .B.1.48 change to:

$$\omega_{800nm} \cdot n_o(\omega_{800nm}) + \omega_{IR} \cdot n_e(\omega_{IR}) = \omega_{SFG} \cdot n_e(\omega_{SFG}) \tag{B.1.49}$$

[2] Thats short for extraordinary wave path + ordinary wave path results into an extraordinary wave path.

Due to the phase matching conditions the following equation has to be fullfilled: $n_e(\omega) = n(\theta, \omega)$. Take care about this as well as calculating all ordinary as well as extraordinary wave paths and put everything into Equ. B.1.49 and solving the now resulted equation with i.e. Mathematica one gets the phase matching angle Θ of approximatly 46°.

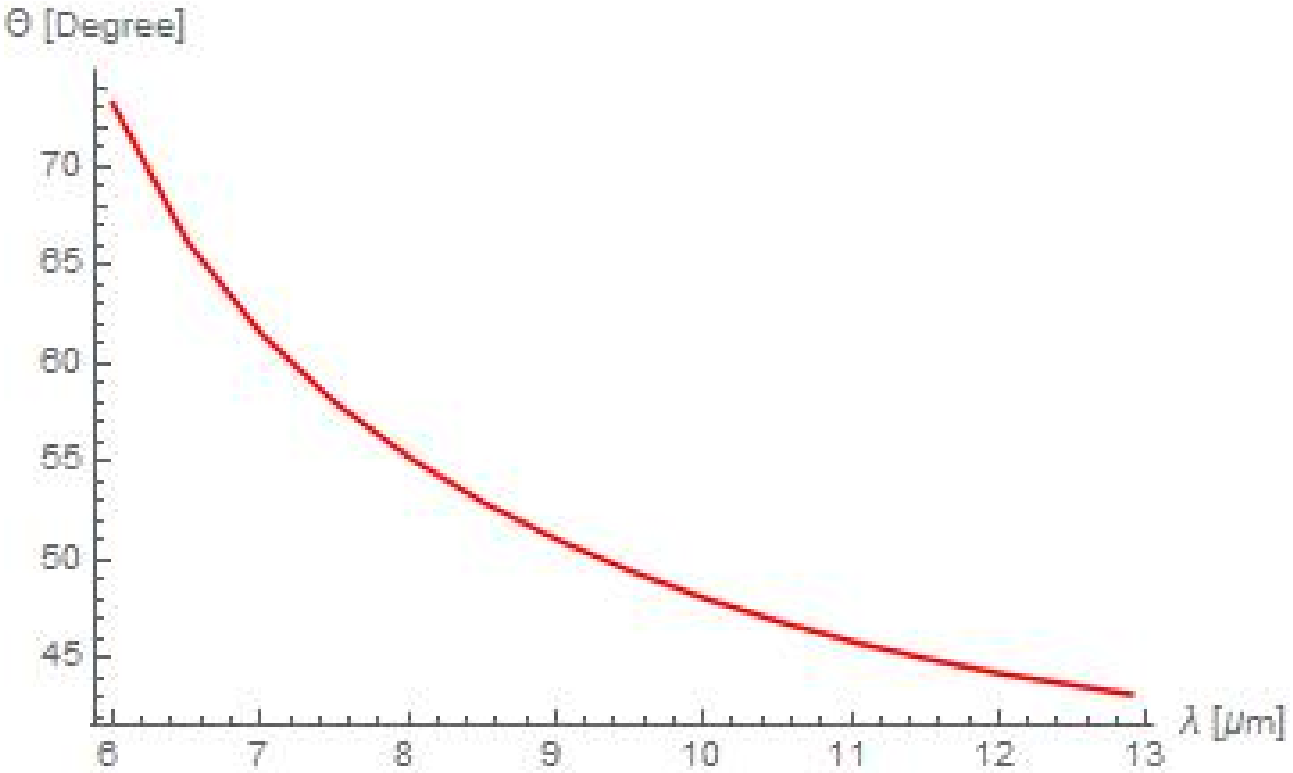

Figure B.1
The calculated refractive index in dependence of the incident beam wavelength λ. Notice that just the wavelength range between $6\mu m$ and $13\mu m$ is shown.

Appendix C

The Zoology Of Pulse Characterisation

In this chapter an extract of up to now developed methods and techniques to measure ultrashort LASER pulses will be shown. Here two different types will be mentioned. On the one hand the interferometric methods and on the other hand the spectrometric one. Both have its own advantages and disadvantages. Which one you need depends on your current task. However, this chapter should be handled as an overview which techniques and methods are available. A detailed description as well as further information you will find in the cited literature as well as are handled in Prof. Rick Trebino's book: [22]. An interessting fun fact is that all of the here mentioned techniques and methods abbreviated represent some animal.

FROG–CRAB The **F**requency–**R**resolved **O**ptical **G**ating for **C**omplete **R**econstruction of **A**ttosecond **B**ursts describes a method for the complete temporal characteriszation of attosecond extrem ultraviolet (XUV) fields [12].

RABBIT The **R**econstruction of **A**ttosecond harmonic **B**eating **B**y **I**nterference of **T**wo–photon **T**ransistions is a method for determination of a detailed temporal structure of XUV pulses [14].

SEA–SPIDER This method is called **S**patially **E**ncoded **A**rrangement for **S**pectral **P**hase **I**nterferometry for **D**irect **E**lectric–Field **R**econstruction of ultrashort optical pulses [21].

SPIDER The **S**pectral **P**hase **I**nterferometry for **D**irect **E**lectric–Field **R**econstruction of ultrashort optical pulses is a self–referencing interferometric technique for measuring the amplitude and the phase of ultrashort pulses. Here a collinear geometry is used as well as a different approach referring the phase–retrieval algorithm [3].

SPIRIT **SP**ectral **I**nterferometry **R**esolved **I**n **T**ime is a self–referencing characteriszation technique for determining the phase as well as the amplitude of ultrashort LASER pulses [23].

TREEFROG This is a method for determining the intensity as well as the phase of two different ultrashort LASER beams. TREEFROG stands for **T**win **R**ecovery of **E**lectric–field **E**nvelope by the use of **FROG** [9].

Bibliography

[1] URL: http://www.ni.com/images/coreblock/large/lvlogo_vert.gif.

[2] Robert W. Boyd. *Nonlinear Optics, 3rd edition*. Academic Press, 2008.

[3] I. A. Walmsley C. Iaconis. "Spectral phase interferometry for direct electric–field reconstruction of ultrahort optical pulses". In: *Optics Letters* (1998).

[4] William H. Press; Saul A. Teukolsky;William T Vetterling; Brian P. Flannery. *Numerical Recipes in C – The Art of Scientific Computing*. Cambridge University Press, 1988.

[5] Markus Werner Sigrist Fritz Kurt Kneubuehl. *Laser*. Vieweg+Teubner, 2008.

[6] David J. Griffiths. *Introduction to Electrodynamics, 3th edition*. Pearson, 2014.

[7] H. J. Eichler J. Eichler. *Laser – Bauformen, Strahlführung, Anwendungen*. 6th. Springer, 2006.

[8] Daniel J. Kane. "Real–Time Measurement of Ultrashort Laser Pulses Using Principles Component Generalized Projections". In: *IEE Journal of Selected Topics in Quantum Electronics* 4 (1998), pp. 278–284.

[9] William E. White Kenneth W. DeLong Rick Trebino. "Simultaneous recovery of two ultrashort laser pulses from a single spectrogram". Version 12. In: *Journal of the Optical Society Am. B.* 12 (1995).

[10] Harald Kirsch. "Chemical reaction on surfaces – a SFG study". PhD thesis. Freie Universität Berlin, 2014.

[11] T. H. Maiman. "Stimulated Optical Radiation in Ruby". In: *Nature 187,493-494* (1960).

[12] Y. Mairesse and F. Quere. "Frequency–resolved optical gating for complete reconstruction of attosecond bursts". In: *Physical Review A 71* (2005).

[13] Wirth Merziger. *Repetitorium der hoeheren Mathematik*. Vol. 5. Binomi Verlag, 2006.

[14] H. G. Muller. "Reconstruction of attosecond harmonic beating by interference of two–photon transitions". In: *Applied Physics B* (Sept. 19, 2001).

[15] David N. Nikogosyan. *Nonlinear Optical Crystals – a complete survey*. Springer Verlag, 2005.

[16] C. W. Peters P. A. Franken A. E. Hill and G. Weinreich. "Generation of Optical Harmonics". In: *Physical Review Letters* 7 (1961), p. 118.

[17] Prof. Dr. Claude Rulliere. *Femtosecond Laser Pulses – Principles and Experiments*. Springer, 2003.

[18] Y. R. Shen. *The Principles of Nonlinear Optics*. Wiley, 2003.

[19] William Thomas Silfvast. *Laser Fundamentals Second Edition*. Cambridge University Press, 2004.

[20] Orazio Svelto. *Principles of Lasers*. 1976.

[21] T. Witting et ali. T. Balciunas. "SEA–SPIDER Characterization of OVER Octave Spanning Pulses in the Mid–IR". In: *Optical Society of America* (2016).

[22] Rick Trebino. *Frequency–Resolved Optical Gating: The Measurement of Ultrashort Laser Pulses*. Springer+Business Media, LLC, 2002.

[23] C. Froehly V. Messager F. Louradour and a. Barthelemy. "Coherent measurement of short laser pulses based on spectral interferometry resolved in time". In: *Optics Letters* (2003).